Journal of Materials Chemistry B

ROYAL SOCIETY OF CHEMISTRY

REVIEW

View Article Online
View Journal

Cite this: DOI: 10.1039/d0tb00990c

Vertical nanowire array-based biosensors: device design strategies and biomedical applications

Xiangling Li,† Jingshan Mo,† Jiaru Fang,† Dongxin Xu,† Cheng Yang, Meng Zhang, Hongbo Li, Xi Xie,* Ning Hu* and Fanmao Liu*

Received 16th April 2020,
Accepted 19th July 2020

DOI: 10.1039/d0tb00990c

rsc.li/materials-b

Biosensors have been extensively studied in the areas of biology, electronics, chemistry, biotechnology, medicine, and various engineering fields. The interdisciplinarity creates an ideal platform for scientists to analyze biological species and chemical materials in a direct, efficient, and sensitive manner; this is expected to revolutionize the life sciences, basic medicine, and the healthcare industry. To carry out high-performance biosensing, nanoprobes – with specific nanoscale properties – have been proposed for ultrasensitive and *in situ* monitoring/detection of tracer biomolecules, cellular behavior, cellular microenvironments, and electrophysiological activity. Here, we review the development of vertical nanowire (VNW) array-based devices for the effective collection of biomedical information at the molecular level, extracellular level, and intracellular level. In particular, we summarize VNW-based technologies in the aspects of detecting biochemical information, cellular information, and bioelectrical information, all of which facilitate the understanding of fundamental biology and development of therapeutic techniques. Finally, we present a conclusion and prospects for the development of VNW platforms in practical biomedical applications, and we identify the challenges and opportunities for VNW-based biosensor systems in future biological research.

1. Introduction

Quantitative detection of biological species and signals plays a central role in many biomedical areas such as understanding disease mechanisms, diagnosing diseases, and developing novel therapeutic strategies.[1] It requires more advanced and accurate sensing techniques to explore deeper life features, which could reveal biological phenomena from the molecular and cellular levels to the organism level. For example, quantitative analysis of the oxygen concentration in the extracellular environment helps in understanding life mechanisms by which cells perceive and adapt to changes in oxygen levels. Dynamic quantitative analysis of intracellular proteins and nucleic acids is also the foundation of the study of cellular life processes.[2–4] The past two decades have witnessed breakthroughs in bio-nanotechnology and its widespread application in the life sciences. As an important and common structure of nanoscale materials, one-dimensional (1D) nanowires have emerged as a powerful tool in multidisciplinary fields on the basis of nano–bio interfaces.[5–8] Bio-detection using vertical nanowire (VNW) array-based sensors is currently a research focus because it can not only meet the increasing demands for high-sensitivity and high-selectivity detection but also provide an ideal platform to detect intracellular information by penetrating the cell membrane, which can hardly be achieved by other biosensors.[9–17]

Studies in the recent decade have demonstrated that VNW arrays, as fundamental tools, can be utilized as nanoscale probes for various applications, such as biosensing,[18–20] electrophysiology,[10,21–24] intracellular matter transfer,[25–29] mechanical transduction,[30–32] and immunomodulation.[31,33,34] Nanowires possess highly tunable parameters, including the optical performance, electrical properties, chemical composition, and topographies. A variety of biochemical sensing techniques can be realized by different surface functionalizations on different nanowires to greatly extend the applications in chemical/biomolecular (H_2O_2, glucose, nucleic acids, proteins, *etc.*) sensing.[25,35–39] Different from free-standing nanowires, VNW arrays enable sensing of multiple cells in a high-throughput and high-spatiotemporal-resolution manner.[40,41] In addition to biomolecular sensing, VNW arrays can also be employed for studying extracellular biophysical signals, including the contraction force and mechanical transduction of cells, because VNWs have a high spatial resolution compared with planar interfaces. Importantly, VNW array-based sensing platforms have been utilized to manufacture devices to sense and stimulate cells.[11,12,24] They could provide attractive opportunities to

The First Affiliated Hospital of Sun Yat-Sen University, School of Biomedical Engineering, Guangdong Province Key Laboratory of Display Material and Technology, School of Electronics and Information Technology, Sun Yat-Sen University, Guangzhou, 510006, China. E-mail: xiexi27@mail.sysu.edu.cn, huning3@mail.sysu.edu.cn, fanmao.liu@foxmail.com

† These authors contributed equally to this work.

simultaneously detect a wide range of biochemical molecules.[42] With good biocompatibility and high controllability, VNW arrays enable minimally invasive operation of cells. The use of patterned VNW arrays could achieve not only the challenging mission of detecting more abundant intracellular signals but also the collection of high-throughput and long-term intracellular signals.[24,43] The VNW arrays with excellent sensitivity are not only derived from the high specific surface area that provide numerous attaching sites for sensing receptors or biomarker molecules or cells, but also the 3D-sensing-matrix guaranteed multichannel detection of weak or spatial-dependent bio-signals. On the other hand, the high selectivity of VNW arrays should partially attribute to the carefully designed geometry and multi-level structure that provides easy binding to specific cell structures such as tentacles and synapses. Additionally, the easy-to-modify bio-recognition layer provides synergistic contribute to the tunable selectivity of VNW.[44]

This review highlights recent advances in VNW array-based biosensors. First, we briefly discuss the development of effective sensing techniques for biomedical information at the molecular level, extracellular level, and intracellular level using VNW-based biosensors and summarize various noncellular applications, including sensing of biomarkers such as RNAs, DNAs, proteins, and other small molecules (H_2O_2, glucose, *etc.*). Moreover, the typical methodologies for detecting extracellular information are discussed, including cellular mechanotransduction and extracellular electrical recording. Second, we reveal cellular behavior by using VNW-based devices in a precise, simple, and comprehensive way owing to the convenient operation at nano–bio interfaces and outstanding biosensor performance. In particular, we review the technologies for intracellular information detection – including both biochemical and electrical sensing – using VNWs to penetrate the cell membrane (Fig. 1). Significantly, this review presents an in-depth understanding of device design strategies for specific biomedical sensing tasks *via* VNW array-based biosensors, and corresponding methodologies. Thus, this review covers several areas of biosensing applications and various VNW materials, differing from reviews focusing on a specific application area or a single material type of nanowires arrays.[13,28] Finally, the development and application directions of VNW arrays in terms of the future prospects of practical biomedical platforms are discussed.

2. Material structures and preparation

2.1 Materials for VNW arrays

At present, research on VNW array-based biosensors is mainly focused on semiconductive and conductive materials, including silicon, silicon oxide, and some metal oxides (*e.g.*, Al_2O_3, TiO_2, ZnO_2, and IrO_2).[14,40,41,45–50] The progress is attributed to the advanced manufacturing technologies established in the micro/nanoprocessing industry.[24] In addition to emerging semiconductor-based nanowire materials, highly conductive gold, platinum, and carbon nanowire arrays also play an important role in constructing biosensors for biological sensing and detection. For instance, research on gold- or platinum-based nanowires has achieved promising progress in the analysis of *in situ* bioactive metabolites and intracellular drug delivery.[51] Recently, in addition to precious metals, carbon nanotubes have achieved real-time detection of reactive oxygen and nitrogen species in the cellular microenvironment.[52]

2.2 Structures and preparation of VNW arrays

Nanowires possess 1D structures, with diameters and lengths ranging from several to hundreds of nanometers.[53] VNW arrays consist of vertically and uniformly distributed nanowires in arrays. The controllable manufacturing routes of VNW arrays are usually divided into two types of method: ''bottom-up'' and ''top-down''.[19] Bottom-up manufacturing involves three steps: packing atoms and molecules along the energy priority direction; assembling NWs from smaller units; and growing materials *via* different routes, including chemical vapor deposition (CVD),[9] the vapor–liquid–solid (VLS) method,[54] atomic layer deposition (ALD),[49] and metal–organic vapor phase epitaxy (MOVPE).[55] In the top-down approaches, VNW arrays are obtained from block materials through advanced engraving or etching processes.[56]

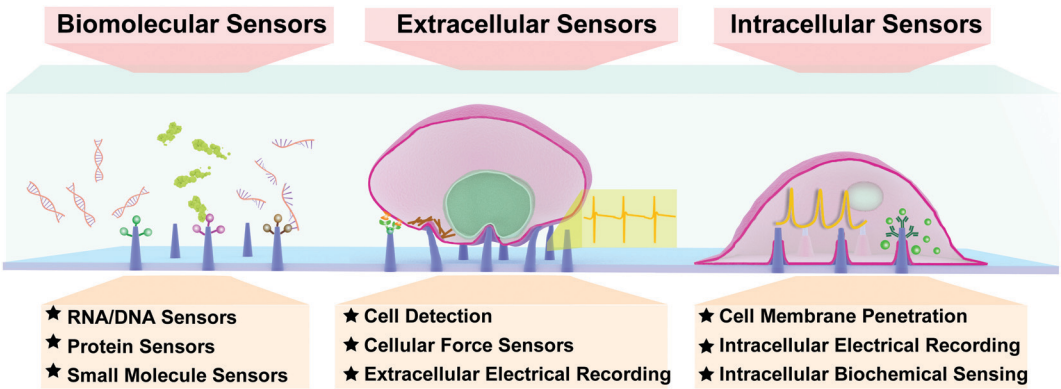

Fig. 1 Illustration of VNW array-based biosensors, covering biomolecular sensing, including of RNAs/DNAs, proteins, and small molecules; extracellular detection, including cellular detection, cellular force sensing, and extracellular electrical recording; and intracellular sensing, including cell membrane penetration, intracellular electrical recording and intracellular biochemical sensing.

These mainly include reactive ion etching (RIE),[57] nonoptical lithography techniques (*e.g.*, electron beam lithography,[58] ion beam e-lithography,[59] X-ray lithography,[60] and interference or holography[61]), and metal-assisted chemical etching (MACE).[56] Nanowire arrays can feature solid, hollow, or hybrid configurations.

2.2.1 Solid nanowire arrays. In 1964, the first small-scale Si microwires were fabricated through a bottom-up synthetic mechanism using VLS technology; however, this early work produced only microscale silicon whiskers or wires.[68] In 1996, Lieber and others began to synthesize SiNWs in a real sense and promoted the concept.[69–72] These advancements provided important insights into controlling the structure and composition of nanowires (GaP, Si, Ge, Ga, Al_2O_3, SiC, *etc.*).[62,73–76] ALD and porous template methods have also been used to prepare solid nanowire arrays (Al_2O_3, ZnO, Si, *etc.*) (Fig. 2a–d).[62–64] In top-down manufacturing, a series of masking steps are usually used to pattern bulk materials. (I) Controllable nanowire (nanopillar) geometric shapes and patterns are obtained by a variety of lithography methods, including UV lithography, colloidal lithography, nanoimprinting, dual-beam focused ion beam (FIB), and electron beam lithography (EBL). (II) The excess materials are selectively removed from patterned substrates *via* an etching step using either a gas or liquid phase (dry or wet etching, respectively), resulting in the formation of VNWs (Si, Pt, *etc.*) (Fig. 2e–h).[66,68]

2.2.2 Hollow nanowire arrays. Different from solid nanowires, hollow nanowires have a unique nanochannel that bridges the extracellular and intracellular microenvironments, facilitating delivery of exogenous cargoes into cells through the nanochannel.[39,40] The template method is a common approach for fabricating nanotube arrays. The typical anodic aluminum oxide (AAO) template method has been used to fabricate nanowire arrays of Ag, Ni, Au, Pt, two-phase composites, and multiphase composites.[77,78] By controlling the electrolyte concentration, current density, and deposition time, well-shaped nanowire/nanotube arrays can be obtained. In addition to the AAO template, polycarbonate (PC) and polyethylene terephthalate (PET) membranes have been used as porous templates to fabricate VNW/nanotube arrays.[79,80]

The fabrication of vertical hollow nanowire (nanostraw) arrays has been reported by Melosh's and Xie's labs.[25,26,40] Typically, metal oxides, such as Al_2O_3, ZnO, and TiO_2, are deposited on porous PC membranes by ALD (Fig. 3a), through which the thickness and composition of thin conformal films can be controlled at the atomic level. The diameter, density, and height of hollow vertical nanostraws can be specified by designing the pore size and porosity of the membranes or by adjusting the power and plasma etching time.

Compared with other deposition techniques (*e.g.*, ALD, CVD and evaporation), electrochemical deposition has great advantages in terms of low cost, easy material treatment, and simple equipment requirements. Electrodeposition allows easy control over the nanotube length, chemical composition (pure or alloy), and uniformity of different types of conductive nanostraws (Fig. 3b).[51] Customized porous template electrodeposition is commonly used to fabricate metal nanostraw arrays.[82]

2.2.3 Hybrid nanowire arrays. With the widespread use of new functional nanowire materials, hybrid nanowire arrays have been developed, which are divided into many elements: segmented doped nanowires, core–shell structures, and spiky nanowires. Different elements will bring about different functional applications of hybrid nanowire arrays. For example, Xu *et al.* reported a hybrid nanowire array-based enzyme-free

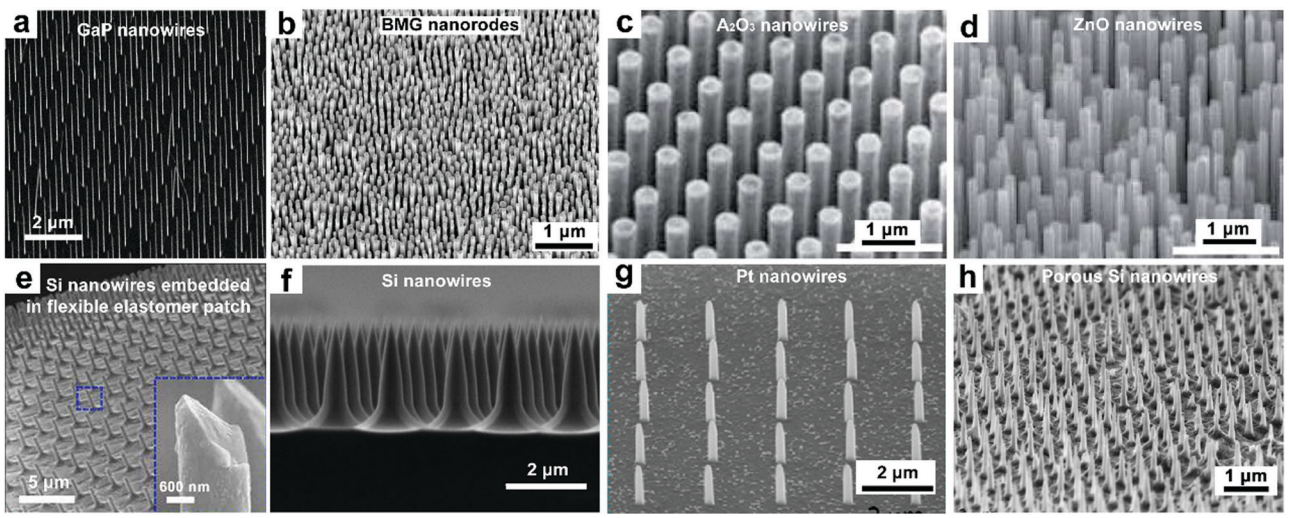

Fig. 2 Overview of vertical solid nanowire arrays of different material types based on scanning electron microscopy (SEM) images. (a) GaP nanowire arrays obtained by the VLS method.[62] (b) Bulk metallic glass (BMG) nanorod arrays (nanorods, not nanorods as in image (b)) obtained by using a porous Al_2O_3 template.[63] (c) Vertical solid Al_2O_3 nanowire arrays obtained by ALD.[64] (d) Vertical solid ZnO nanowire arrays obtained by ALD.[64] (e) Si nanowire array partly embedded in polydimethylsiloxane (PDMS).[65] (f) Cross-section of vertically aligned Si nanowire arrays.[34] (g) Square 5 × 5 Pt nanopillar array obtained by FIB.[66] (h) Vertical solid porous Si nanoneedle array obtained by RIE.[67] Reproduced with permission from ref. 34 and 62–67 copyright (2010) and (2014) American Chemical Society Publishing Group, (2019) The Royal Society of Chemistry Publishing Group, (2018) American Association for the Advancement of Science, (2019) Wiley-VCH Publishing Group, and (2010) and (2015) American Chemical Society Publishing Group.

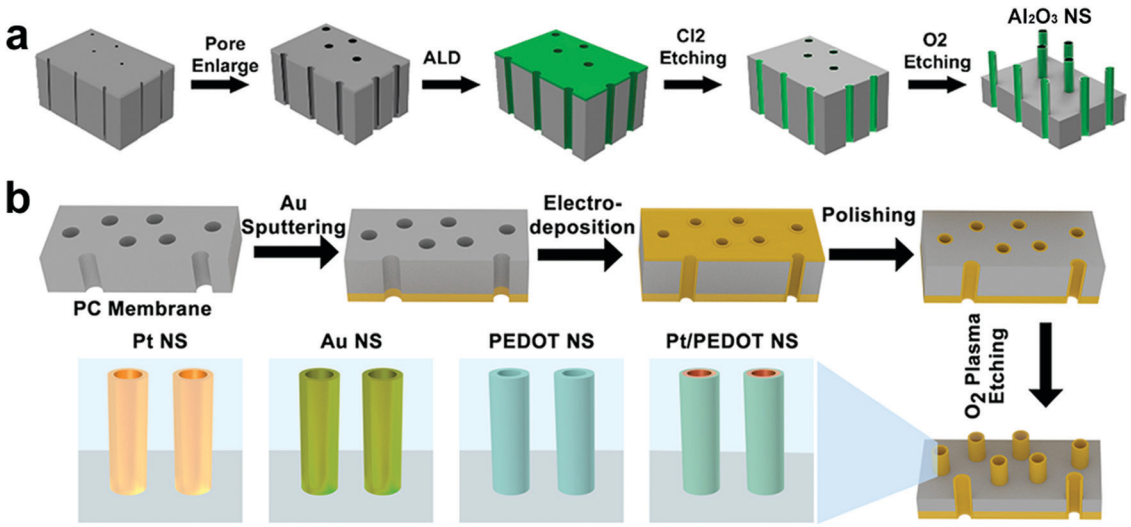

Fig. 3 Schematic of vertical hollow nanowire (nanostraw) arrays fabricated by ALD (a) and electrochemical deposition (b). Reproduced with permission from ref. 51 and 81, copyright (2018) and (2019) American Chemical Society Publishing Group.

glucose biosensor. Ni nanoparticle doping in TiO_2 nanowire arrays improved the sensitivity by shortening the electron and ion transfer distance in the nanowire array biosensor (Fig. 4a).[83] Unlike multielement doped nanowire arrays, core–shell nanowires (Fig. 4b) are combined in a coaxial cladding with a significantly heterogeneous structure, which can achieve functional complementarity of various materials and improve electrophysiological signal recording. For example, core–shell VNW electrode arrays were used for intracellular electrophysiological recording (Fig. 4c).[24,85] Inspired by the bionic structure of the extracellular matrix (ECM), spiky nanowire arrays, such as ZnO or ITO arrays, were developed; when combined with specific antibodies, these spiky nanowires promoted effective capture of circulating tumor cells (CTCs) (Fig. 4d and e).[86,87]

Repeatability of VNW arrays based sensors relies on two major aspects: the reliability of the physical structure of nanowires, the stability of the bio-recognition layer attached on the surface of nanowires. The influence factors of the former aspect include the material of nanowires that metal and semiconductor nanowires generally possess higher mechanical reliability than metal oxides, the processing method which "top-bottom" strategies lead to higher mechanical reliability than "bottom-up"

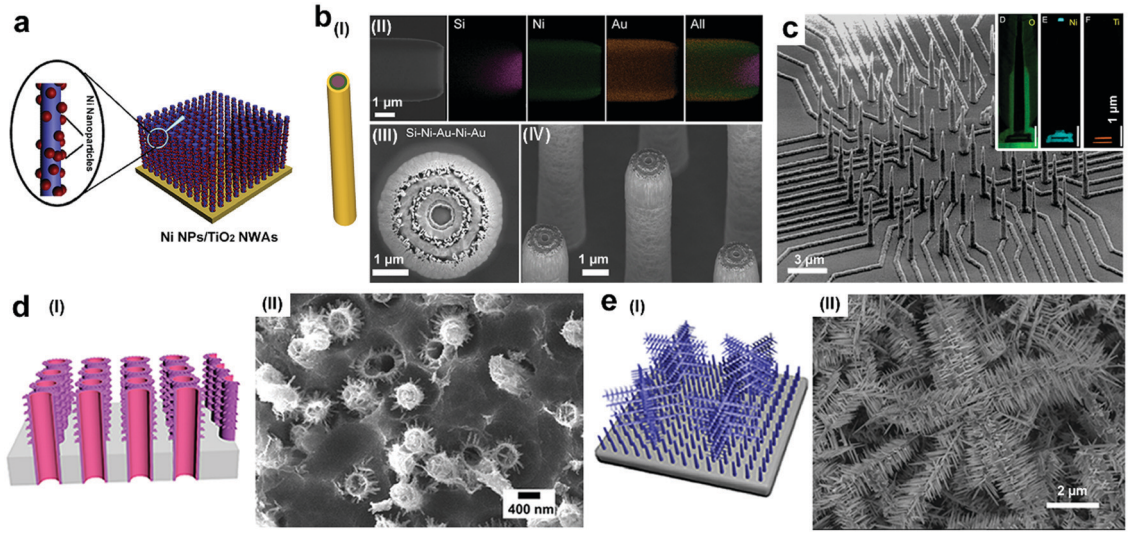

Fig. 4 Overview of hybrid nanowire arrays. (a) Schematic diagram of Ni nanoparticle doping in TiO_2 nanowire arrays.[83] (b) Schematic (I) based on scanning transmission electron microscopy (STEM) images. The top right illustration shows the corresponding elemental maps (II), and the bottom right shows SEM images of Si–Ni–Au coaxial nanowires (III and IV).[84] (c) SEM image and energy-dispersive X-ray spectroscopy (EDX) results of electrically isolated nanowire probes after SiO_2 passivation.[85] (d) Schematic (I) and SEM image (II) of multifunctional branched nanostraw arrays.[44] (e) Schematic (I) and SEM image (II) of ITO-III nanowire arrays.[86] Reproduced with permission from ref. 44 and 83–85, copyright (2017) Elsevier Publishing Group and (2017), (2017), (2019) and (2016) American Chemical Society Publishing Group.

method, the complexity of the structure where hollow nanowires, core–shell nanowires, spiky nanowires, *etc.* result in easier structure failure than simple solid nanowires structure. The latter aspect is mainly depended on how the bio-recognition layer bonds to the nanowires, in which chemical bonding methods brings higher stability than physical approaches such as dip coating and spin coating. On the other hand, each strategy that improves the repeatability of VNW sensors generally lead to certain disadvantages, for instance, "top–bottom" processing method requires costly equipment and complex procedures, simple solid nanowires limits the sensitivity and selectivity to specific cell structures, chemical bonding procedures imply more technological parameters to tune and control. Therefore, choosing proper materials, structures and preparation methods in designing a VNW sensor for specific biomedical application is always needed.

3. Biomolecular sensors

Biomolecules are closely related to biological activity. DNAs, RNAs, proteins, and other biologically active small molecules (*e.g.*, H_2O_2 and glucose) have been selected as biomarkers to predict or diagnose diseases at the early stage. Accurate detection of biomolecules has become a wide problem of concern in the biomedical field. However, due to the wide variety and low concentrations of biomolecules, performing highly sensitive and selective detection is difficult. To solve this problem, advanced biosensors based on VNW arrays have been developed.[35,37,88–113]

3.1 RNA/DNA sensors

As the carrier of genetic information, DNA contains the core information related to life and disease. In 1985, Mullis developed the polymerase chain reaction (PCR) method to amplify DNA, which is of great significance for clinical and scientific research.[114] However, PCR is a time-consuming method that has difficulty meeting the requirement of rapid detection. Recent studies have shown that VNW arrays, with highly specific surface areas, provide an effective method for rapid DNA detection.[110,115–117] To date, several DNA nanowire-based sensors have demonstrated different detection mechanisms, such as photonic resonance, fluorescence, the electrical diode effect, photoluminescence, and cyclic voltammetry (CV) (Table 1).

Lu and coworkers fabricated a photonic crystal nanowire array device by combined top-down and bottom-up processes. They used EBL to prepare SiNW arrays on a SiO_2 substrate and then sputtered a gold layer onto the SiNW array surface. Target dsDNAs were hybridized to single-stranded probe DNAs, and the resonant frequency linearly shifted with the target dsDNA concentration (500 aM–10 pM, Fig. 5a). Nucleotide modification can enhance the surface doping effect of SiNWs, which increases the induced current and improves the detection sensitivity of the biosensor. In addition, Kim and coworkers developed a diode-type biosensor using a vertical silicon nanowire array, on the topside of which graphene was coated.[105] A 27 bp oligonucleotide from the human DENND2D promoter sequence was decorated as probe DNA on the AuNP@SiNW layer. The hybridization of the NW arrays increased the current in the biosensor owing to the enhancement of the doping effect of the SiNW surface. As the concentration of target DNAs varied from 100 pM to 500 nM, the current of the biosensor increased from 19% to 120%. This device showed great performance in endurance tests and appeared to be an accurate, selective, and stable biosensor (Fig. 5b).

RNAs serve as a bridge between DNAs and proteins and control the expression of genetic information in proteins. Modern medicine has discovered different expression (down-regulation/overexpression) levels of RNAs between patients and healthy people. Lee and coworkers demonstrated the detection of HIV-1 Rev response element (RRE) RNA by gold-coated silicon nanowire arrays. A factitious peptide sequence was used as the probe to connect target RNAs and the gold surface. The peak CV electric current showed a prominent decline after immobilization of RRE RNAs, linearly corresponding to the RNA concentration from 1.513 fM to 20 fM.[106] Yasui *et al.* designed a device for efficient *in situ* extraction of urine extracellular vesicle (EV)-encapsulated miRNAs, which bind to ZnO nanowires on PDMS substrates with a herringbone microfluidic channel.[109] *Via* an electrostatic collection mechanism, this device can collect among 1000 kinds of miRNAs from urine at an extremely low concentration of EVs. Importantly, these miRNAs could serve as biomarkers for urologic cancer and other diseases (Fig. 5c).

Nanowires can be employed not only to accurately identify DNAs and RNAs but also to separate DNAs, RNAs, and proteins of different sizes. For example, Rahong *et al.* demonstrated a

Table 1 Key characteristics of nanowire systems for DNA/RNA detection

Materials & structure	Target	Height (μm)	Diameter (nm)	Mechanism	Concentration range	DNA copies range (copies per mL)	Limit of detection	Ref.
Au@SiNWs	DNA	1.7	100	Photonic resonance	500 aM–10 pM	10^2–10^6	—	91
AuNPs@SiNWs	DNA	2	170	Fluorescence	>50 pM	$>10^6$	—	93
APTES@SiNW network	DNA	10	70–100	Fluorescence	0.1–1 μM	10^{12}–10^{13}	—	96
Graphene@SiNWs	DNA	0.3	50	Electrical diode effect	0.1 pM–1 μM	10^4–10^{11}	—	105
AuNRs@GaAsNHs	DNA	0.316	89 (top) 302 (bottom)	Photoluminescence	1 pM–50 nM	10^5–10^9	1 pM	110
Au-Nanorods (AuNRs)	DNA	—	100	CV	10 fM–10 nM	10^3–10^8	10 fM	113
Au-Nanoneedles	DNA	—	100	CV	0.2 fM–10 nM	10–10^8	0.2 fM	113
Au@SiNWs	RNA	1	100	Differential pulse voltammetry (DPV)	1–20 fM	~40–10^3	1.5 fM	106

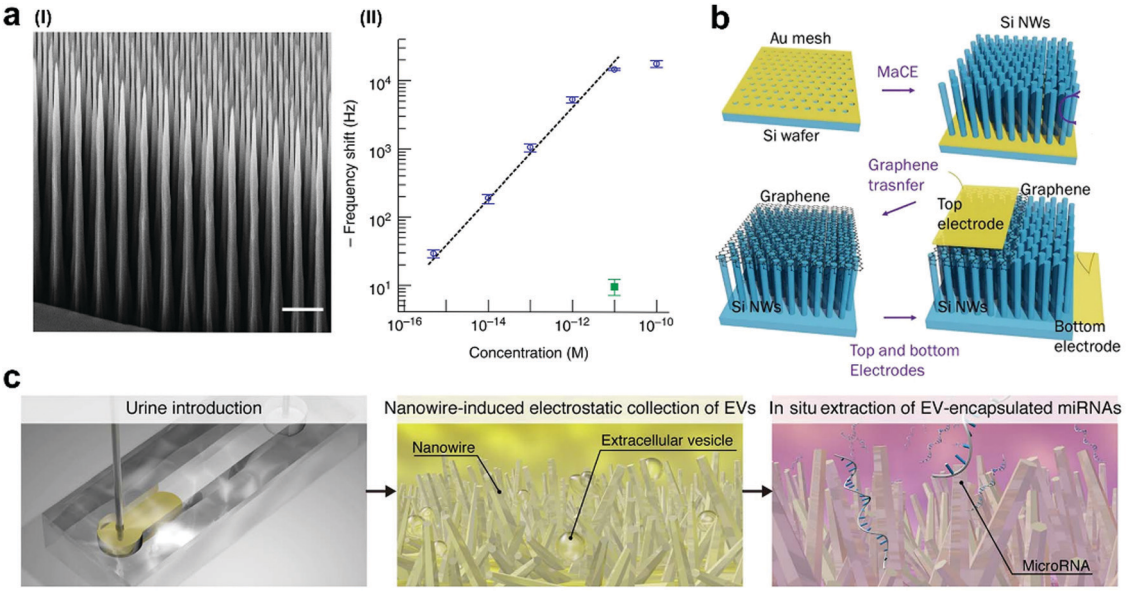

Fig. 5 Nanowire arrays for DNA/RNA detection. (a)-(I) SEM image of a SiNW array. (II) Linear frequency response to the DNA concentration. (b) Schematic diagram of the fabrication process of vertically aligned SiNW arrays. (c) Schematic illustrations of miRNA collection. Reproduced with permission from ref. 91, 105 and 109, copyright (2011) Springer Nature Publishing Group, Reproduced under the terms of the Creative Commons Attribution NonCommercial License 4.0. Copyright (2018), The Authors, Published by Springer Nature Publishing Group and (2017) American Association for the Advancement of Science Publishing Group.

rigid three-dimensional (3D) network structure for ultrafast analysis of DNAs with sizes from 100 bp to 166 kbp; they fabricated multibranched nanowires within a microchannel. A fabrication cycle included catalyst deposition and nanowire growth, where smaller branched nanowires grew on stem nanowires after each cycle.[100,103,104] Accordingly, the mode pore size was decreased to match the target DNA size. An electrophoresis experiment showed that DNAs with different sizes have relatively different mobilities in the microchannel; this feature was utilized for DNA size analysis and separation (Fig. 5c).

Compared to Real-time Quantitative PCR (qPCR), the widely used laboratory technique for dynamic analysis of nucleic acids, particular VNW based sensor can achieve LOD low to the magnitude of 10 copies for specific DNA segments,[113] that is close to the LOD of qPCR (2–10 copies) in practice. While in most cases it is believed that qPCR possesses higher sensitivity than VNW based sensors at present. On the other hand, VNW based DNA/RNA sensors with electrical sensing mechanism have significant advantage in the response time due to the "true" real-time electrical signal recording, rather than the qPCR technique that multi-step temperature regulations are required. Thus it can be expected the wider application of VNW based DNA/RNA sensors with more stable performance and uniform protocols.

3.2 Protein sensors

Proteins are a major category in the life sciences; they include tissue proteins, enzymes, antibodies, and hormones. Protein detection has great significance for proteomics and clinical applications. Application of VNW arrays has demonstrated the possibility for protein detection at a low concentration, which could promote early disease screening based on protein biomarkers. Protein detection mechanisms based on VNWs can be divided into two categories: label-based methods and label-free methods. Label-based methods including fluorescence[118] and luminescence[110] perform high specificity to targets with simple operation and reliability, while request costly fluorescent or luminescent agents for marking and be lack of dynamic detection capability. Label-free methods of VNWs based protein detecting mainly refers to electrical methods (*e.g.* cyclic voltammetry, piezoelectric, FET), which electrical indications are dynamically related to target protein molecules. Take the case of the most common utilized label-free method, cyclic voltammetry was restricted to its narrow linear range and high limit of detection (LOD) in early researches.[89,90] Recent works reported a broad linear range and low LOD even to aM magnitude to specific proteins, demonstrating VNWs based protein sensing as a competitive candidate with common standard methods such as enzyme-linked immunosorbent assay (ELISA) and proximity ligation assay (PLA), which generally offers detection range from pM to nM.[110,111]

Effective simultaneous detection of multiple targets has always been a concern. Han and coworkers separated SiNWs into several patterns using the walls of microwells made of PEG hydrogel.[95] SiNWs were modified with AuNPs and glutaraldehyde to enhance the protein absorbability. A double microchannel model was used for simultaneous fluorescence detection of IgGs and IgMs, with high sensitivity and selectivity. Theoretically, this device can be developed into high-throughput microchannels for bioassays (Fig. 6a). A protein sensor is usually based on antigen–antibody coupling. Corresponding antigens are generally conjugated to the primary NW surface. Target proteins

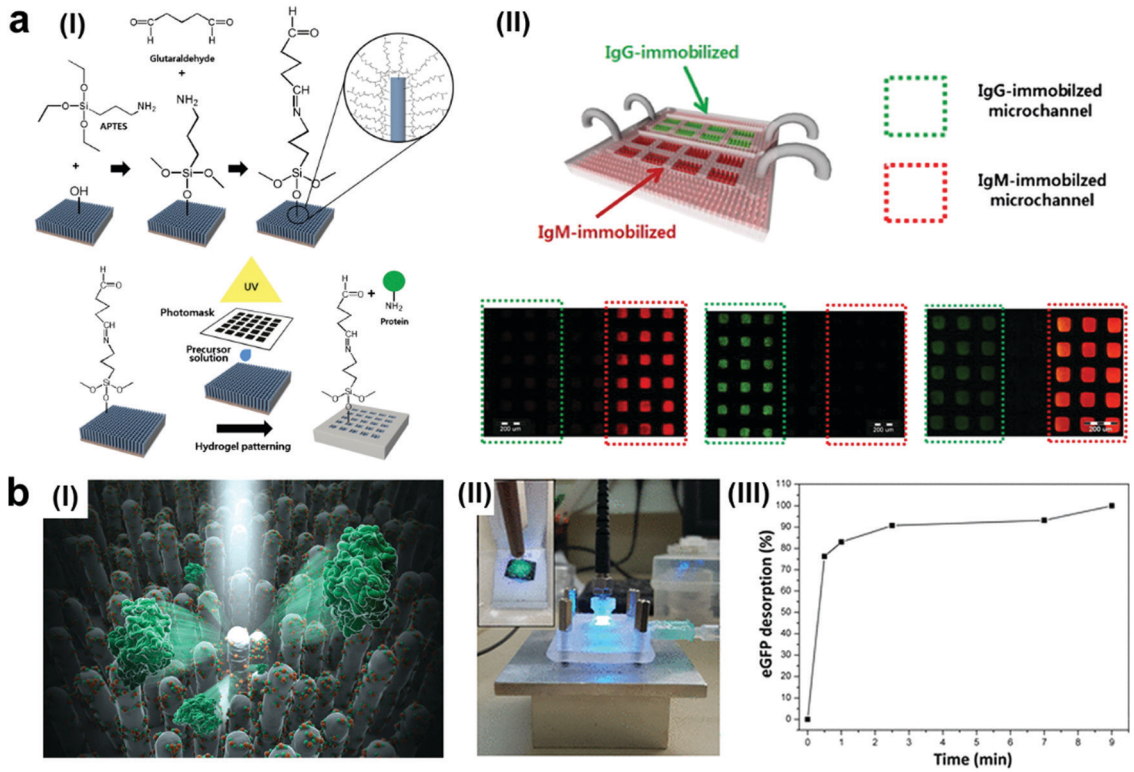

Fig. 6 Nanowire arrays for protein detection. (a)-(I) Schematic illustration of protein immobilization by SiNWs. (II) Simultaneous detection of different proteins by microchannels. (b)-(I) Schematic illustration of protein movement by light control. (II) Photo of a light-controlled SiNP device. (III) eGFP desorption rate over time. Reproduced with permission from ref. 38 and 95, copyright (2013) and (2019) Elsevier Publishing Group and American Chemical Society Publishing Group, respectively.

attach to VNW arrays due to the affinity of materials or by chemical conjugation. For example, gold is one kind of biocompatible material and is used as a modification material (AuNPs and Au coatings)[89,90,99,110] and a nanowire material.[103] The work listed in Table 2 used a pretreated sample solution with only a single target protein or a few contrast proteins. However, those devices are not capable of directly detecting proteins in blood samples that contain more than 10^4 different proteins. Ella Borberg *et al.* demonstrated a revolutionary light-controlled Si nanopillar (SiNP) array for selective adsorption and desorption of proteins.[35] First, target proteins were absorbed into the cavities of the SiNPs due to the affinity of modified antibodies. After the blood sample was removed, a light-triggered pH drop on the surface of the SiNPs converted the surface affinity for proteins from ultrareceptive to ultrareflective, resulting in a rapid release of target proteins. This work offered a method to selectively collect low-concentration proteins by removing undesired blood components. Importantly, the selective nanowires could be integrated into a sensor array, realizing the detection of proteins in complex samples (Fig. 6b).

3.3 Small-molecule biomarker sensors

Other small molecules (*e.g.*, H_2O_2 and glucose) are also key physiological indicators for the relevant state in an organism. H_2O_2 is involved in a variety of biological events and intracellular pathways and is associated with a variety of diseases, such as cancers and diabetes. Quantitative analysis of H_2O_2 in biological environments is helpful for better understanding the

Table 2 Key characteristics of nanowire systems for protein detection

Materials & structure	Target	Height (μm)	Diameter (nm)	Mechanism	Concentration range	Limit of detection	Ref.
AuNPs@SiNWs	BSA	—	250	CV	3–7 μM	1.4 μM	89
AuNPs@SiNWs (APTES)	BSA	2–2.5	100	CV	1–7 μM	—	90
Microwells of SiNWs	IgG	8	150	Fluorescence	50–100 and 100–1000 ng mL^{-1}	10 ng mL^{-1}	95
Microwells of SiNWs	IgM	8	150	Fluorescence	10–100 and 100–1000 ng mL^{-1}	1 ng mL^{-1}	95
Au@ZnONWs	Immunoglobulins	0.18	78	Piezoelectric effect	50 ng mL^{-1}–1 mg mL^{-1}	102 ng mL^{-1}	99
Hollow AuNWs	Tob	2.5	300	CV	10 fM–1 nM	3 fM	118
AuNRs@GaAsNHs	Tob	0.316	89 (top) 302 (bottom)	Photoluminescence	10 pM–10 nM	10 pM	110
ZnO nanorods	HBsAg	1.54	228	FET	20 aM–1 pM	20 aM	111

Table 3 Key characteristics of nanowire systems for small molecule detection

Materials & structure	Target	Height (μm)	Diameter (nm)	Mechanism	Concentration range	Sensitivity [μA (mM cm^2)$^{-1}$]	Limit of detection	Ref.
PtNPs@AuNWs	H_2O_2	6	200	Amperometry	0.02–20 mM	194.60	1.0 μM	88
PtNPs@AuNWs	Glutamate	6	200	Amperometry	0.2–1.6 mM	10.76	—	88
$Ni(OH)_2$@SiNWs	H_2O_2	80	100	Amperometry	0–5.5 mM	3.31	3.2 μM	94
CuO@SiNWs	H_2O_2	12	200	Amperometry	0.01–13.18 mM	22.27	1.6 μM	35
PtNWs	H_2O_2	12	200	Amperometry	0.01–4 mM	654	2.4 μM	129
Cu_2O@TiNTs	H_2O_2	—	—	Amperometry	0.5–8 mM	412.11	90.5 μM	108
AuNPs@TiO_2NWs	Glucose	—	200–210 (outer) 120 (inner)	Amperometry	0.4–8.0 mM	—	0.31 mM	92
Cu_2O@TiO_2NTs	Glucose	—	105 (outer) 85 (inner)	Amperometry	3.0–9.0 mM	14.56	62 μM	98
Au–Ni coaxial NRs	Glucose	30	150 (Au) 250 (Ni)	Amperometry	0.0275–27.75 mM	778.2	5.5 μM	97
Au@SiNWs	Glucose	0.25–0.4	70	Amperometry	55.1 μM–16.53 mM	390.5	11 μM	101
CuONPs@ZnONRs	Glucose	1.2	80–90	Amperometry	0.001–8.45 mM	2961.7	0.4 μM	37
CoNiCuNTs	Glucose	2	280	Amperometry	50–1551 μM	791	0.5 μM	112
CoNiCuNTs	Glucose	2	280	Amperometry	1551–4050 μM	322	0.5 μM	112

metabolic mechanisms of life and the changes in oxygen levels in related biological diseases. Accurate quantification of the blood glucose concentration is a direct reflection of the blood glucose level. At present, titration,[119,120] fluorescence,[121,122] chemiluminescence,[123,124] spectrophotometry,[125,126] electrochemistry,[127,128] and other analytical techniques have been applied to the determination of H_2O_2 and glucose. Among them, electrochemical sensors based on VNW arrays possesses the advantages of fast response, high sensitivity, and good selectivity (Table 3).

H_2O_2 detection is mainly based on metal or metallic oxide-modified materials that promote the decomposition of H_2O_2, which produced electrons transfer that alter electrical current. Nanowires act as the adsorption and conduction units. Metal nanowire arrays demonstrate greater sensitivity than SiNW arrays, but Si is more economical than Au and Ti. Huang *et al.* chose CuO as an electrocatalyst material for selective H_2O_2 detection.[35] SiNWs were prepared by chemical etching with the supplement of predeposited AgNPs. The AgNPs were then removed, and Cu nanoparticles (NPs) were distributed on the SiNWs by electroless deposition. Finally, CuONP-modified SiNWs were formed after thermal oxidation. This device demonstrated a sensitivity of 22.27 μA (mM cm^2)$^{-1}$ for H_2O_2 detection with a linear increase from 0.01 to 13.18 mM and the LOD of 1.6 μM (Fig. 7a). Ahmad *et al.* demonstrated an ultrasensitive glucose sensor with a ZnO nanorod (NR) array modified with CuONPs (CuONPs@ZnONRs).[37] ZnONRs were grown on fluorine-doped tin oxide (FTO) electrodes by a hydrothermal method, followed by CuONP deposition. With the great electrochemical and catalytic properties of CuONPs, the device demonstrated an ultrasensitivity of 2961.7 μA (mM cm^2)$^{-1}$ for glucose detection with a linear range from 0.001 to 8.45 mM and low LOD of 0.4 μM (Fig. 7b).

VNW arrays can also be applied for the detection of other micro-biomolecules. Kim *et al.* fabricated Au-decorated ZnONRs (Au@ZnONRs) for the diagnosis of three types of eye diseases (cataracts, age-related macular degeneration, and diabetic macular edema).[129] ZnONRs were grown on a flexible graphite sheet by the hydrothermal method, and the gold layer was deposited by E-beam evaporation. When adding aqueous humor from patients with different eye diseases into the device, the spectrum of the surface-enhanced Raman scattering (SERS) appeared different. Such a device demonstrated the potential of VNW arrays in clinical applications (Fig. 7c).

A common ground could be found among various biomolecular sensing applications of VNW arrays is that all nanowire electrodes were connected at the substrate rather than working individually. The physical forms of VNW arrays are closer to planar electrodes with multiple sub-electrodes integrated superficially, and those wire-electrodes are generally with diameters over 100 nm, far from threshold dimension of the nano-size effect (usually $<$10 nm). Thus, the impedance of VNW arrays would be reduced only due to the increased specific surface area than the planar electrodes, and be no significant different from a single micro/nano-wire on a unit surface area. Excellent sensing performance of VNW arrays on biomolecules is likely to be more from the decorated functional nanostructures with at least one dimension close to or smaller than 10 nm, especially the modified AuNPs which occupied the most reports in Tables 1–3. Here VNW arrays play the important role in the system that provides massive attaching sites of the bio-recognition nanostructures in specific sensing area and demonstrates the spatial distribution of sensing signals.

The ''bulk nanowires'' design strategy that all nanowire electrodes connected at the substrate to form an integrated electrode rather than multiple individual nanowire electrodes, significantly reduces the fabricating complexity of VNW sensors. Moreover, normal solid nanowires without multi-level structures such as spikes can meet the requirement of detecting target biomolecules in liquid samples in most cases. And the most successful design strategy of VNW sensors for biomolecular detecting should be the employment of Au-based nanostructure as the sensing interface. Advantages of Au-based nanostructure in biosensing includes facile fabrication, highly tunable geometry, specific catalytic and optical properties, highly sensitive to light, high conductance and specific surface area, excellent

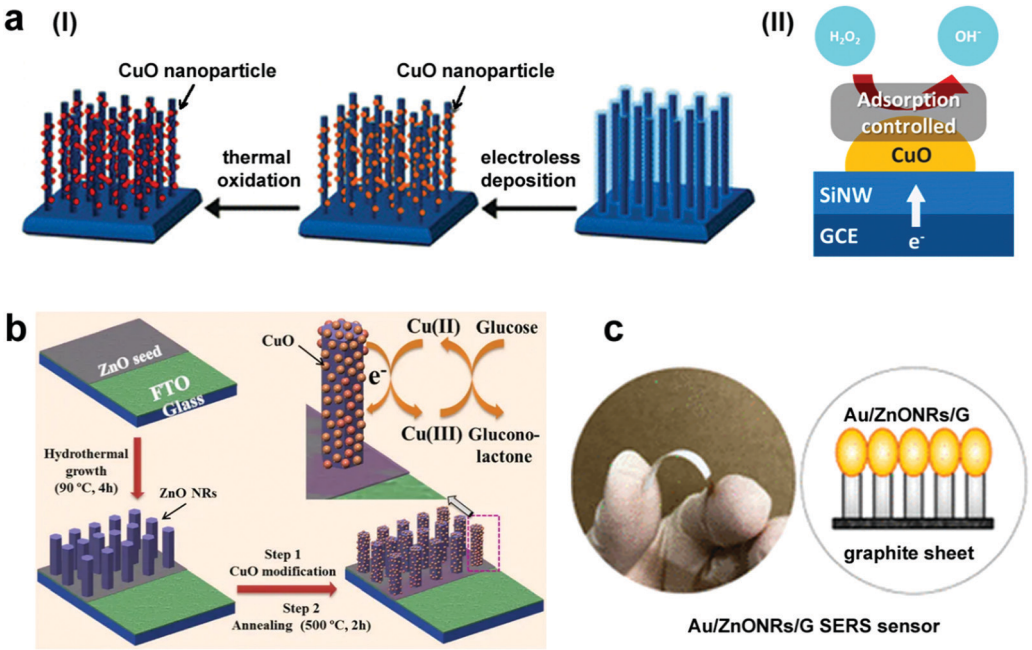

Fig. 7 Nanowire arrays for small molecule sensors. (a) H_2O_2 sensors: (I) schematic illustration of the immobilization of CuO on a SiNW array. (II) Mechanism for H_2O_2 detection. (b) Glucose sensors: schematic illustration of the generation process and detection mechanism of the glucose sensor. (c) Other small molecule sensors. Reproduced with permission from ref. 35, 37 and 129, copyright (2014), Reproduced under the terms of the Creative Commons Attribution NonCommercial License 4.0. Copyright (2017) American Chemical Society Publishing Group and Elsevier Publishing Group, respectively.

biocompatibility, strong bonding to nanowires, *etc.* Pt and Cu based nanoparticles were also utilized as sensing interface *via* similar strategy. All these contributions greatly raise the potential of VNW sensors as future universal tools for dynamic analysis of biological samples.

4. Extracellular sensors

Extracellular sensors provide insights into cellular behavior such as cell differentiation and proliferation, which are critical for the early diagnosis of disease, understanding biological mechanisms, and developing new therapeutic strategies.[130] Extracellular sensing includes the detection of CTCs, cellular electrical signals, and mechanotransduction sensing.

4.1 Cancer cell sensors

The detection of CTCs and other abnormal cells is of great significance for the early diagnosis and treatment of malignant tumors. However, due to their limited number in peripheral blood, efficiently detecting target tumor cells by traditional methods is difficult.[131] In recent years, nanowire arrays have been proposed to capture and analyze CTCs.[132,133] Nanowire arrays have a large specific surface area, providing sufficient binding sites for specific molecular recognition and improving the cell-capture efficiency. Furthermore, the topological interaction between nanowire array structures and cell surfaces can vastly improve the cell-capture affinity and facilitate the identification of abnormal cells in whole blood.[134] Wang and coworkers have presented seminal reports on an efficient cell-capture platform based on 3D nanostructured substrates.[135] The results demonstrated a higher cell-capture efficiency on Si nanopillar arrays (45–65%) compared with that on flat Si substrates (4–14%). The platform was then integrated into a chaotic system of microfluidics, and the cell-capture efficiency was improved to 90% by the synergistic effects of the enhanced cell–substrate interaction intensity and frequency (Fig. 8a).[136] Moreover, high-density gold nanocluster (AuNC)-coated SiNWs demonstrated an even higher capture efficiency. Park and coworkers reported a SiNW surface covered by single-monolayer, high-density, and highly uniform AuNCs through rapid thermal CVD.[137] After 40 min of cell incubation, the capture efficiency for breast cancer cells on the antibody-coated AuNC–SiNW surface reached ~88%, which is almost twice that of pure SiNWs. Alternatively, increasing the hierarchical structure of ITO nanowire arrays is a novel strategy to improve the capture efficiency. Zhang *et al.* fabricated a new 3D fractal nano–bio interface with horizontal and VNW branches. This fractal nano–bio interface obtained an 89% capture efficiency for EpCAM-positive cells within 35 min of incubation (Fig. 8b),[86] which is significantly higher than the 67% efficiency within 45 min obtained by an ITO nanowire array without branches.

Inspired by the cell microenvironment, Liu *et al.* reported soft polystyrene nanotube (PSNT) substrates coated with a specific recognition molecule that can efficiently capture breast cancer cells (Fig. 8c).[133] The cell-capture efficiency of the soft PSNT substrates was 80%, higher than those of smooth

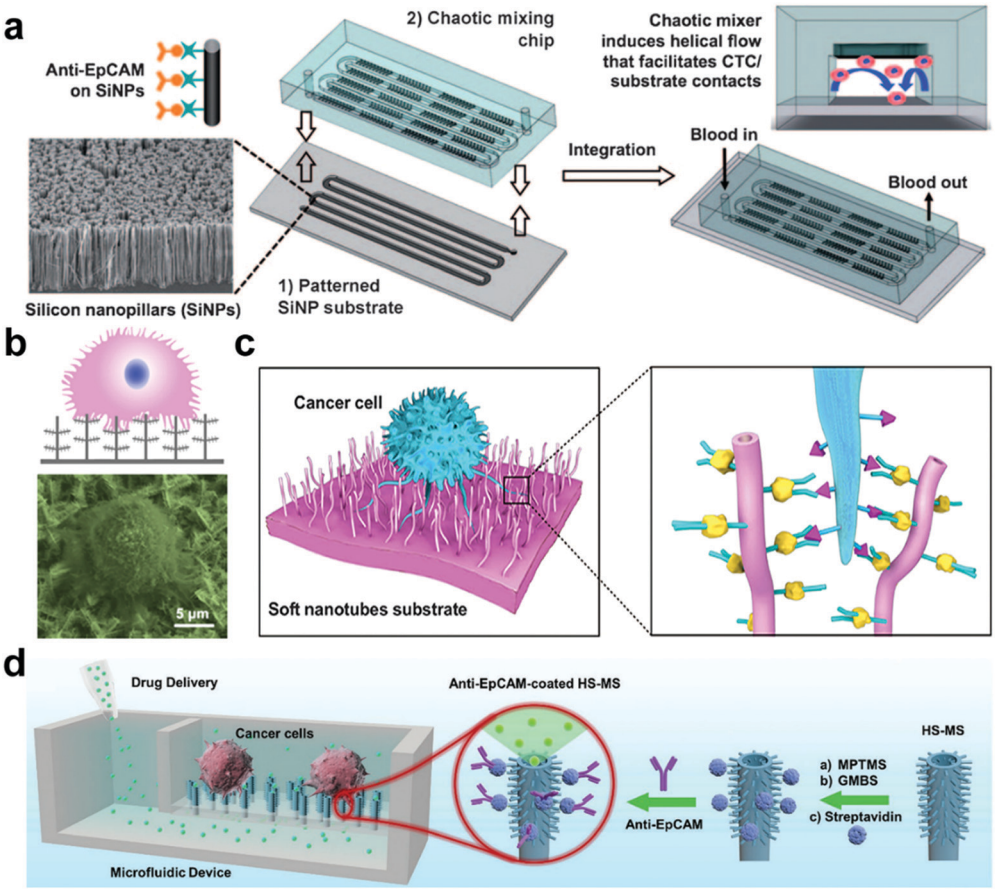

Fig. 8 VNW arrays for cancer cell detection. (a) Integrating SiNP arrays into a microfluidic chaotic mixing system. (b) Schematic illustration and environmental SEM (ESEM) image of ITO nano–bio interfaces capturing cells. (c) Schematic illustration and ESEM image of cancer cell capture by a soft nanotube substrate. (d) Schematic illustration of a hierarchical spiky microstraw-integrated microfluidic device for capture of cancer cells and *in situ* manipulation of the captured cells. Reproduced with permission from ref. 86, 133, 136 and 138, copyright (2011) Wiley-VCH Publishing Group, (2016) American Chemical Society Publishing Group, (2013) Springer Nature Publishing Group and (2019) Wiley-VCH Publishing Group, respectively.

PS substrates (~50%) and inorganic rigid SiNW systems (~40–60%). The softness of such platform materials is conducive to future biological research and applications. 3D VNW arrays have great advantages in cell capture; however, drug delivery, intracellular extraction, and *in situ* regulation of cells cannot be realized due to the limitation of their structures. Recently, He and coworkers developed a microfluidic device integrated with hierarchical spiky hollow nanowire (nanostraw) arrays (Fig. 8d).[138] The hierarchical spiky hollow nanostraw arrays were demonstrated to be able to effectively capture cancer cells and carry out *in situ* chemical operations. Furthermore, multifunctional branched hollow nanostraw arrays combined with an electroporation system were used to extract intracellular contents with excellent spatiotemporal control capability.[139]

As an integrated device, arrays of nanowires can achieve excellent space and time control and multi-dimensional detection of biomolecules or cells, especially multi-cell batch operation, which is obviously not available for single nanowires. Regarding the sensitivity and selectivity of detection, efficient CTC capture and specific identification of CTC and other cells are achieved through the treatment of VNW, including the common physical spines and chemical coating of specific antibodies.

4.2 Electrical sensing

Electrical signal recording data are considered to be a key indicator of excitable cell physiology. The monitoring of electrical signal changes in cardiomyocytes and neurons could facilitate investigation of human life behavior and its biological basis and could promote further development of biomedical research and clinical studies. Conventional extracellular detection usually uses field-effect transistors (FETs). For example, electrolyte–oxide–silicon (EOS) FETs can record electrical signals of individual mammalian neurons.[140] However, this two-dimensional (2D) structure has a low coupling degree between cells and electrodes, thus giving a low signal quality. With the development of micro/nanosensor detection technology, a platform for high-sensitivity, high-resolution, and high-throughput synchronous recording of electrical signals has been developed using VNW arrays.[141]

3D VNW array-based biosensing electrodes possess the advantages of 1D, 2D, and 3D structures: the 1D single

nanowire structures create a coupling between electrodes and cells; the 2D planar substrates realize multichannel monitoring of signals; and the 3D spatial structures and bionic patterns provide a large specific surface area to contact cells. Inspired by the particle phagocytosis phenomena of living cells, 3D electrode structures can induce phagocytosis, forming a good seal and increasing neuron–electrical coupling. Mimicking the dimensions of dendritic spines, Aviad Hai *et al.* fabricated 3D gold microstructures, which could be readily engulfed by cultured cells after being functionalized with peptides (Fig. 9a).[142] In comparison with flat electrodes, 3D gold-spine electrodes were tightly coupled with cells and significantly increased the field potential signals. The 3D electrode structure intrinsically had a large surface area, which could reduce the electrode impedance and increase charge transfer at a given electrode diameter.

In addition, coating nanowires with highly conductive nanomaterials, such as carbon nanotubes (CNTs), is considered an effective way to improve signal recording. Taking advantage of this feature, coating conventional metal electrodes with CNTs can further enhance neuron recording and electrical stimulation while maintaining chemical inertness and biocompatibility (Fig. 9b).[143] The CNT coatings prepared by the electrochemical deposition method provide variable geometry and electrochemical properties, leading to the development of brain–computer interface devices. 3D electrodes are usually based on traditional conductors, and the mechanical cues from electrodes will be converted into biochemical signals that affect cell activity. Interestingly, an electrically conductive hydrogel (ECH) is another ideal candidate material for preparing mechanically matched electrodes due to its softness and compatibility with cells and tissues. Liu *et al.* fabricated an ECH micropillar electrode based on poly(3,4-ethylenedioxythiophene) polystyrene sulfonate (PEDOT:PSS), which was modified with a highly conductive ionic liquid (Fig. 9c).[144] The ECH micropillar electrode can obtain a higher signal-to-noise ratio (SNR) and a stronger signal intensity than the conventional iridium oxide micropillar electrode. Moreover, the electrode has better mechanical compatibility with cells, reducing the influence of mechanical forces on cells.

4.3 Mechanotransduction sensing

In addition to regulation of cancer cells and recording of extracellular electrical signals, VNW arrays can also be used to detect the mechanical properties of cells. The mechanical properties of a substrate, especially the stiffness, can be sensed by

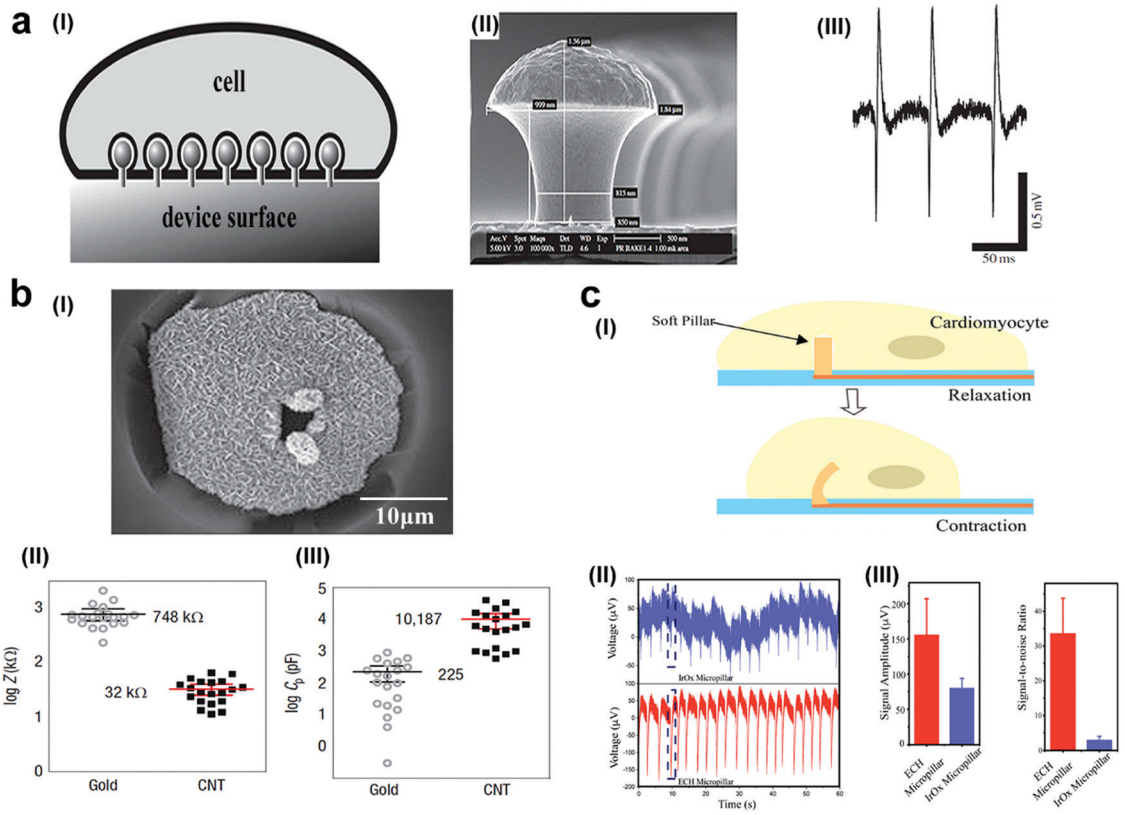

Fig. 9 Detection of extracellular electrical signals using VNW arrays. (a)-(I and II) Schematic illustration and SEM image of gold spines. (III) Potential signals recorded by a four-gold-spine electrode. (b)-(I) SEM image of a CNT-coated electrode. (II and III) Impedance decreases and charge transfer increases after CNTs are coated. (c)-(I) Schematic illustration of a soft multielectrode array for electrophysiological recording. (II and III) Comparison of extracellular recordings, signal amplitudes and SNRs of iridium oxide micropillar and soft ECH micropillar electrodes. Reproduced with permission from ref. 142–144, copyright (2009) Royal Society Publishing Group, (2008) Springer Nature Publishing Group and (2018) Proceedings of the National Academy of Sciences Publishing Group, respectively.

adherent cells through integrin-mediated mechanotransduction, resulting in an intracellular stress field that affects cell behavior and functions. In the study of cell mechanotransduction, an elastic micropillar system can be used to detect the subcellular forces by monitoring the surface wrinkles caused by cell contraction. However, micropillars have large pillar diameters and spacings, which limit the spatial resolution of cell movement and force. In contrast, nanowires have the advantages of a high filling density, a nanoscale size, and a wide stiffness range, all of which can be used to better study molecular signal sensing and mechanotransduction of cells. By combining traditional photolithography with deep RIE, Yang and coworkers designed nine different nanopost arrays with diameters ranging from 0.75 to 1.5 μm and center-to-center spacings ranging from 1.5 to 4.5 μm (Fig. 10a).[145] The cell diffusion on the nanopost surfaces was similar to that on planar continuous substrates. Four of nine nanopost arrays were suitable for traction force measurement, and the strain energy of each cell in the different arrays was constant; such nanopost arrays have the potential to measure the mechanical energy output of cells. Recently, P. Paulitschke *et al.*

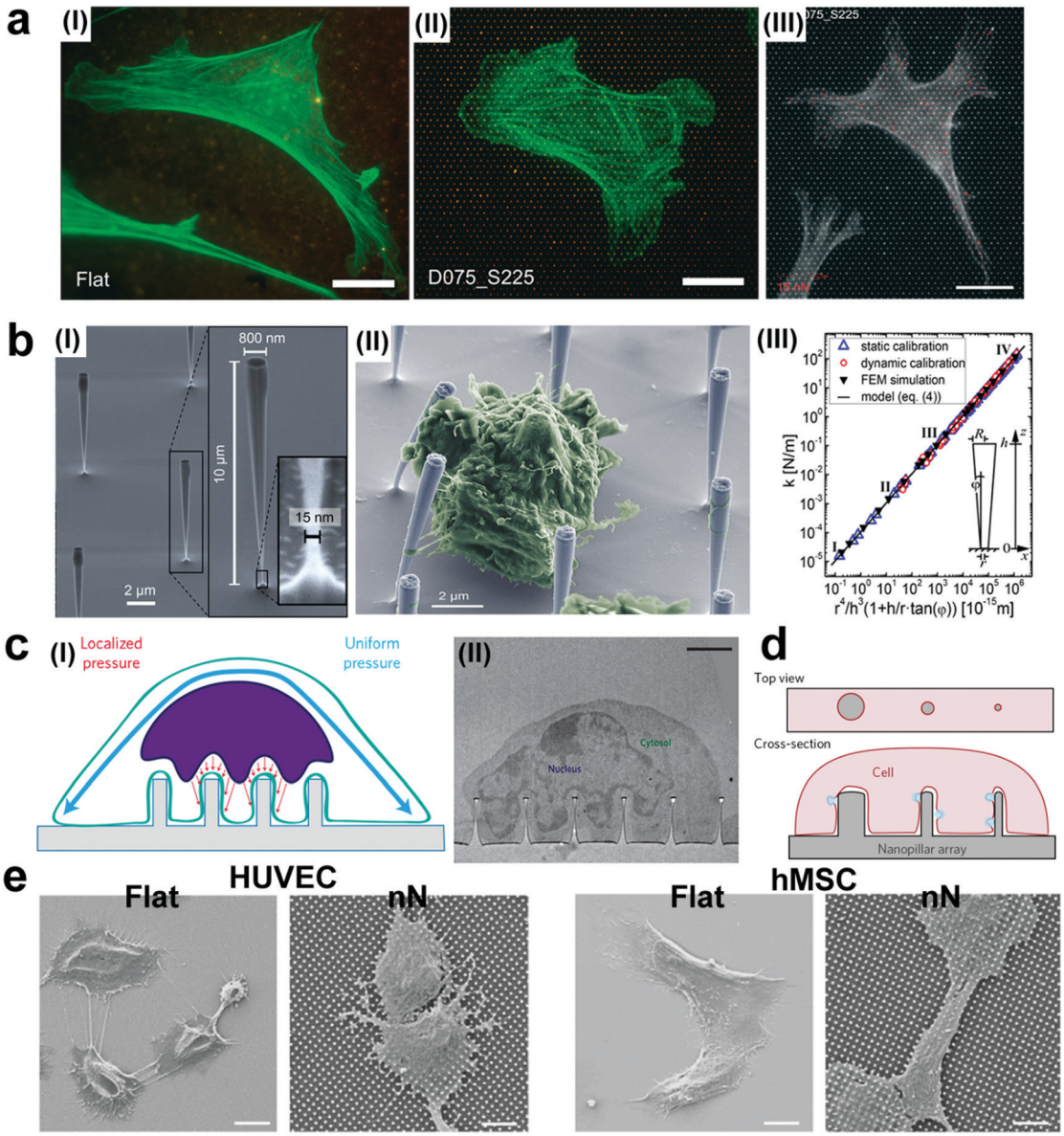

Fig. 10 Cell mechanotransduction sensing with VNW arrays. (a)-(I–III) Images and force vector plots of cells on nanopost surfaces. (b)-(I) SEM images of cellular force sensors and GaAs nanowires. (II) SEM image of a cell confined by a VNW array. (III) Mechanical characterization and COMSOL Multiphysics simulation of GaAs nanowire arrays. (c)-(I) Illustration of the cell-VNW array mechanical model; (II) TEM image of a nucleus deforming around a nanopillar array. (d) Schematic illustration of nanopillars with different radii deforming a cell membrane with different curvatures. (e) SEM comparative images of cells after direct interaction with nanoneedles for 6 h. Reproduced with permission from ref. 30, 32 and 145–147, copyright (2007) Wiley-VCH Publishing Group, (2019) American Chemical Society Publishing Group, (2015) and (2017) Spring Nature Publishing Group and (2019) American Chemical Society Publishing Group.

developed an ultraflexible nanowire array biosensor composed of inverted conical semiconductor nanowires with a small spring constant that could improve the cell force detection sensitivity.[146] In this system, light was reflected from the nanowires and propagated only through the buffer solution. The light path was totally separated from the cells, which prevented cell-induced optical distortion while obtaining information on cell-induced mechanical effects. The resolution of the cell-induced force detection with the ultraflexible nanowires could reach 50 pN and even 100 fN, which is conducive to the realization of high-sensitivity, high-resolution, unlabeled, and distortion-free biosensors for optical microscopy detection (Fig. 10b).

Recent studies have shown that the mechanical properties of the nucleus and its mechanical coupling with the cell membrane are essential for cell migration, polarization, proliferation, and gene expression. The nanoscale topography can cause significant deformation of the cell membrane and nuclear membrane, affecting cellular behavior. Cui's group fabricated regular arrays of vertical quartz nanopillars for noninvasive research on the live nuclei deformation ability. The results indicated that nuclear deformation was affected by the nuclear stiffness, actin, and intermediate filaments (Fig. 10c).[30] VNW arrays for research on nuclear mechanical transduction and nuclear deformation effects on cellular behavior and for gene expression research provide a unique platform. This group recently fabricated vertical SiO_2 nanopillars, which can be enveloped by a plasma membrane, producing membrane curvatures ranging from +50 to −500 nm; these membrane curvatures directly regulate the biochemical activity of clathrin-mediated endocytosis (CME) proteins. The local accumulation of CME proteins was significantly increased under the guidance of membrane curvatures of less than 200 nm; some CME-related proteins, such as clathrin and dynamin, had more significant changes under the action of a positively curved membrane (Fig. 10d).[147] Further studies have shown that nanoneedle arrays can be used as intracellular mechanoresponsive elements. More recently, Stevens' group reported mesoporous silicon nanoneedle arrays with a high aspect ratio. The nanoneedle arrays interacted with cell membranes and inhibited focal adhesion maturation; they also noninvasively and reversibly interacted with actin networks and the nucleus to reduce the cytoskeletal tension and displace the nuclear envelope, which stimulated the dynamic remodeling process of lamin proteins. Mechanically stimulated reconstruction can be achieved at the organelle level by further modification of the nanoneedle arrays (Fig. 10e).[32]

Summarized information of representative VNW arrays for extracellular sensing application were categorized in Table 4, including materials, geometries, processing methods, biomedical applications and performances. It can be found that the ''bulk nanowires'' design strategy is still widely utilized to achieve good balance between the device fabricating complexity and extracellular sensing performance. And top-down approach that mainly refer to physical/chemical etching was involved in fabricating almost all reported VNW sensors for extracellular sensing, as it provides better mechanical strength of nanowires than bottom-up approach. This can be considered as the strategy to adapt the mechanical condition when nanowires contact the cell. Moreover, nanowires with superficial multi-level structures were employed for enhance the contacting sites to cell membrane and specific cell structure such as tentacles or synapses, which can improve the efficiency of cell capture and optimize the quality of electrical signal. Other methods include the general use of anti-EpCAM antibodies to recognize and capture CTCs, appearance of flexible polymer nanowires for a better mechanical match with cells, and so on. All these considerations promote the development of VNW sensors towards powerful extracellular sensing platform.

5. Intracellular sensors

5.1 Cell membrane penetration approaches

Compared with extracellular detection, intracellular detection can obtain more accurate information about living cells. Nanowire array-based sensors can penetrate the cell membrane and enter the intracellular compartment; these sensors can transfer a variety of biological molecules and detect intracellular electrical and biochemical signals.[22,148]

To conduct intracellular detection, spontaneous and/or assisted cell membrane penetration methods help the nanowire array-based biosensor pass through the cell membrane and directly contact intracellular signals. Spontaneous penetration has been observed during intracellular delivery when biomolecules attached to VNW arrays were successfully delivered into cells through the membrane. However, spontaneous penetration of nanowires into a cell membrane is a rare event with a probability of ~7%.[41,149] Nano–bio interfacing is more likely to cause endocytosis rather than spontaneous penetration. A study reported by Cui's group claimed that membrane curvatures and accumulation of endocytosis-related proteins in living cells were controlled by nano-3D structures.[147] CME regulates the distribution of membrane proteins and allows extracellular mediators to enter the cell. To improve the membrane penetration efficiency by nanowire arrays, four methods have been applied, namely, electroporation, photoporation, chemically modified penetration, and mechanical penetration.

Electroporation is the most commonly used method in facilitating nanowire-mediated penetration. For bulk electroporation, cells are suspended between two parallel electrodes with hundreds to thousands of volts applied. However, because VNW arrays are in close contact with cells, a much smaller voltage (approximately 1–3 V) is sufficient to generate a large electric field – comparable to that in bulk electroporation – around the nanoscale interface (Fig. 11a).[10,51] Alternatively, Dipalo *et al.* proposed that photoporation can induce transient nanopores in cell membranes.[150] It uses 3D vertical micro- and nanostructures to improve the signal quality of multielectrode arrays and open nanopores without damaging the seal between the membrane and the nanowires (Fig. 11b). Spontaneous reorganization of the membrane occurs within a few minutes and ends without side effects. For chemically modified penetration,

Table 4 Summary of VNW arrays used for extracellular sensors applications

Material	Geometry	Height (μm)	Diameter (nm)	Fabrication method	Cell type	Capture mechanism	Biomedical application	Performance[a]	Ref.
Polystyrene	Nanotube	—	~200	AAO template, NaOH etching	MCF7, PC3, T24, HeLa, Jurkat T, Daudi	Modified by anti-EpCAM	Detection of CTCs	~80%	132
Si	Nanopillar	1–20	100–200	Wet chemical etching	MCF7	Modified by anti-EpCAM	Detection of CTCs	45–65%	134
Si	Nanopillar	12–15	100–200	Wet chemical etching, soft-lithography	MCF7	Modified by anti-EpCAM, microfluidics system	Detection of CTCs	90%	135
Si	Nanoneedle	3–4	600 (base), 100 (apex)	Low-pressure CVD, MACE, RIE	HUVECs	Stimulation of cell mechanotransduction machinery	Mechanotransduction	Reversibly organelle remodeling	32
Au, Si	Gold clusters on silicon nanowires	5–10	50–160	RTCVD	MCF7	Modified by anti-EpCAM	Detection of CTCs	~88%	136
ZnO	Hierarchical spiky microstraw array	~1.5	1 μm	ALD, RIE, hydrothermal approach	MCF7	Modified by anti-EpCAM	Detection of CTCs	~84%	137
ITO	Hierarchical nanowire	—	—	Multistep CVD	MCF7, PC3, HeLa	Modified by anti-EpCAM	Detection of CTCs	~89%	86
ZnO, TiO_2	Branched nanostraw	1–2	~400	ALD, RIE, hydrothermal growth	MCF7	Modified by anti-EpCAM	Detection of CTCs	~93%	138
Au	Mushroom-shaped spine	1 μm stem	800 nm stem, 1.8–3 μm cap	Photolithography, electrodeposition	Neurons	Modified by engulfment promoting peptide	Cellular electrical signals	770 ± 294 μV	141
PEDOT:PSS	Micropillar	1.8 (dry)	3 μm	Electron beam evaporation, ion milling, plasma-therm versaline oxide etching	Cardiomyocytes	Mechanically matched electrodes	Cellular electrical signals	~156 μV	143
PDMS	Nanopost	3	0.75–1.5 μm	Photolithography, RIE, template method	NIH/3T3	Traction force experiments	Mechanotransduction	—	144
GaAs	Nanowire	10	800	EBL, ICP-RIE	Dictyostelium discoideum	Cell-induced forces	Mechanotransduction	Resolution of 50 pN	145
SiO_2	Nanopillar	0.7–2	100–700	EBL, RIE	NIH3T3	Nuclear mechanics	Mechanotransduction	Controlling the geometrics of nuclear deformation	30
SiO_2	Nanopillar	0.7	100–1000	EBL, RIE	SK-MEL-2	Manipulation of membrane curvature	Mechanotransduction	Examining ten CME-related proteins	146
GaP	Nanoneedle	1.5, 3.8, 6.7	80	MOVPE	Mouse fibroblasts	—	Cellular behaviors	—	4

[a] Performance: percentages stand for CTCs capture efficiencies; potentials stand for magnitudes of electrical signals; texts present effects of the rest applications.

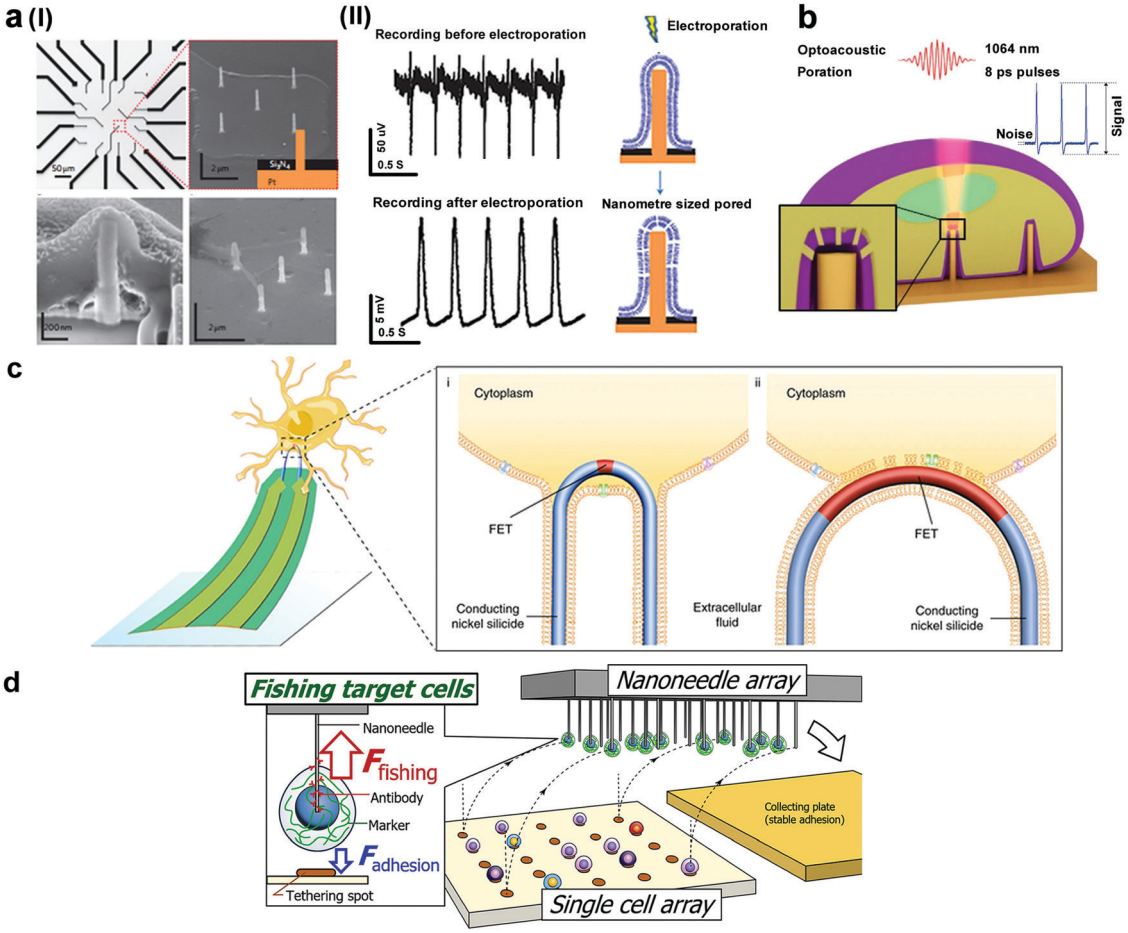

Fig. 11 Methods of penetrating the cell membrane. (a)-(I) Recording the signal using an electrode with a four-by-four array of platinum sheets and a diameter of ~150 nm, observed under SEM. (II) Action potentials before and after electroporation of a single HL-1 cell was recorded, showing different signal amplitudes. After electroporation, the voltage pulse formed nanopores in the cell membrane. (b) Schematic diagram of the transmission of nanowires into living cells using a photoactivatable nanowire endoscope. (c) A 3D U-shaped nanowire FET adjusts the nanoscale curvature so that sensors can record intracellular signals across cell membranes. (d) Schematic diagram of cell-specific separation by mechanical penetration of antibody-functionalized nanoneedles. Reproduced with permission from ref. 10,22,151,152, copyright (2012) Nature Publishing Group, (2019) Wiley Publishing Group, (2019) Nature Publishing Group and (2017) American Chemical Society Publishing Group, respectively.

cells allow drugs to enter by endocytosis or fusion of the phospholipid bilayer on the membrane. Nanoscale curvature of the cell membrane increases the local accumulation of endocytosis proteins, affects the conformation and activity of transmembrane proteins, and recruits a series of proteins[12,147] that cause membrane splitting (Fig. 11c) – all contributing to probe internalization and intracellular recording.[151] In addition, Kawamura *et al.* provided an alternative method of penetrating the membrane using mechanical penetration to separate different types of cells. In this method, multiple antibody-functionalized nanoneedles were inserted into multiple cells to achieve specific separation of a single cell from mixed cells (Fig. 11d).[152]

5.2 Detection of intracellular electrical signals

Action potentials play an important role in a number of processes involving changes in ion channels. The higher the coupling between cell membranes and electrodes is, the more accurately the action potential can be measured. Electrode-based methods of measuring membrane action potentials make further research in neuroscience and cardiology possible.[21] Two approaches to recording cellular electrical signals currently exist: extracellular and intracellular. Extracellular signal detection can be performed without crossing the cell membrane; for instance, a multielectrode array can be used for long-duration and multi-channel detection. However, this recording method cannot provide a one-to-one cell-to-electrode correspondence, so the signal strength and quality are greatly reduced.[23] Intracellular electrical signal detection, such as diaphragm clamping, can be achieved by using electrodes to measure changes in the voltage or current intracellularly and extracellularly. At high SNRs, this method can faithfully record the amplitude and shape of electrical signals. Intracellular detection is invasive and has a shorter recording time. Because of its complexity, it cannot record signals from more than one cell simultaneously.[24] Therefore, the use of VNW arrays is an ideal method for detection with the least cell damage. Different from traditional intracellular electrophysiological probes, VNW arrays can

measure intracellular electrical signals without causing ion exchange, minimizing the interference with biochemical reactions. Furthermore, their nanoscale dimensions can reduce cellular destruction and biological toxicity.[10,11,153]

VNW electrode arrays (VNEAs) can record intracellular signals, stimulate neuronal activity in separately cultured rat cortical neurons, and map out the synaptic connections of individual neurons. Robinson *et al.* reported that the VNEA platform was easily integrated with conventional fluorescence microscopy and photogenesis techniques, allowing for multiple detection of neurons. The small size and planar geometry of VNEAs help their integration into implantable electrodes, opening up new possibilities for high-fidelity interfaces with hundreds of individual neurons and studies of neural circuit dynamics (Fig. 12a).[11] Lin *et al.* extended the sustainable time of the channel by optimizing the geometry of the intracellular nanometer electrode channel to improve the amplitude of measured electrical signals.[45] The design of vertical iridium oxide (IrO_x) nanotube electrodes promotes spontaneous membrane wrapping around the outside of the nanotubes and the center of their protruding site (Fig. 12b). A CMOS integrated circuit combined with a nanoscale intracellular electrode was applied to horizontal parallel recording of intracellular networks and electrophysiological imaging (Fig. 12c). The CMOS nanometer electrode array consisted of a 1024 pixel array (32 × 32) that can simultaneously record intracellular potentials from hundreds of newborn rat ventricular cardiomyocytes. Electrical signals can be produced by electroporation through voltage pulses.[24] In their very recent work, these researchers reported an array of nanoscale electrodes containing 4096 platinum black electrodes and nanoscale silicon

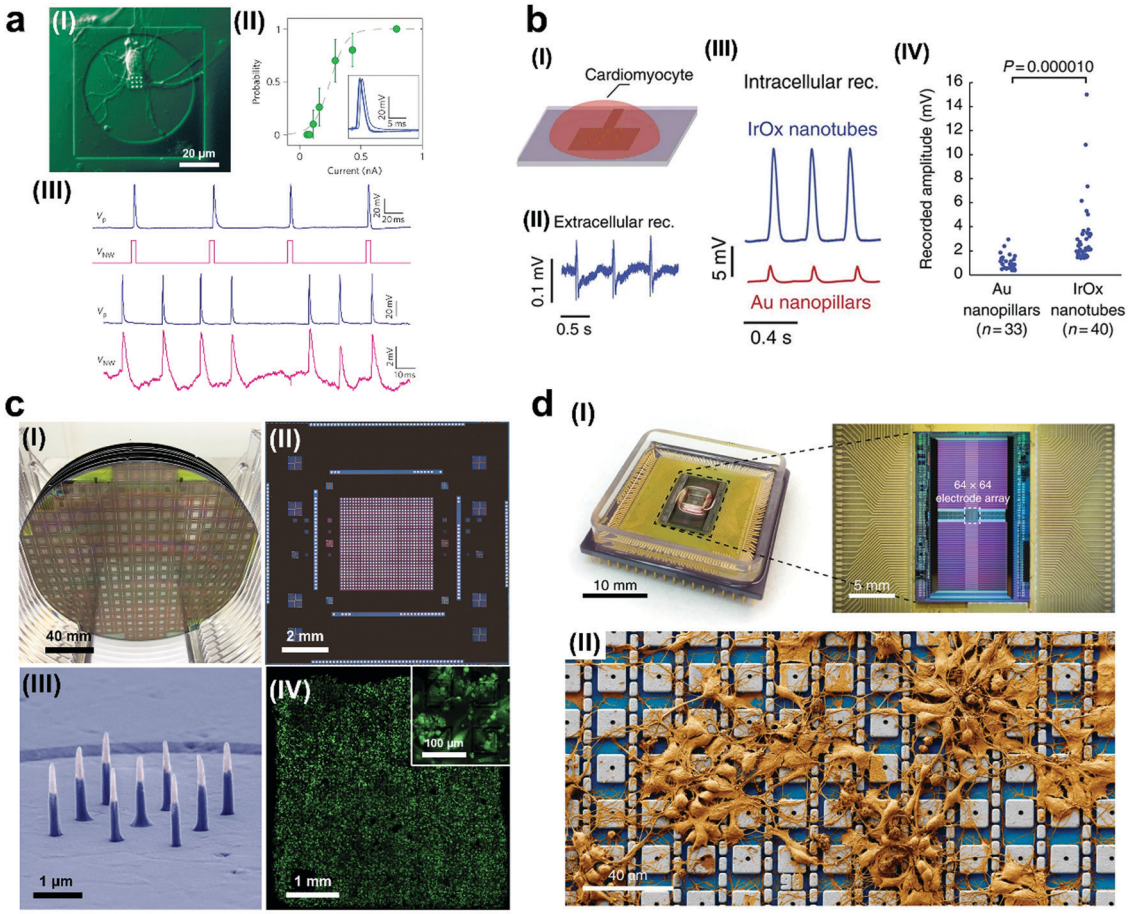

Fig. 12 Detection of intracellular electrical signals using VNW arrays. (a) Recording and stimulation of rat cortical neurons by VNEAs. (I) Photomicrograph of a rat cortical neuron cultured on a VNEA. (II) The action potential excitation probability function shows an s-shaped dependence (dotted line). Illustration: five consecutive chronological action potentials excited by current injection of nanowires. (III) Use of a voltage pulse (magenta) on the VNEA to stimulate the action potential and a patch pipette (blue) to record the action potential. (b)-(I) Recording of the action potential with an IrO_x nanotube electrode. (II) The extracellular action potential of HL-1 cardiomyocytes was measured before electroporation. (III) After electroporation, both IrO_x nanotubes and Au nanopillars achieved intracellular action potential recording. (IV) Statistical results showing that the signal recorded by the nanotube electrodes is much larger than that by the nanopillar electrodes with similar surface areas. (c)-(I) CMOS nanometer electrode array. (II) Integrated circuit centered on a 32 × 32 pixel array. (III) False-colored SEM images of the 9 vertical nanometer electrodes produced for each pad. The top of the electrodes is Pt exposed, and the bottom is SiO_2 insulated. (IV) Fluorescence image of cardiomyocytes cultured in the equipment (stained with calcein-AM). Green represents living cells. (d)-(I) Photos of a CMOS-activated PtB nanoelectrode array that contains 64 × 64 pixel pads. (II) False-colored SEM image of cells cultured on top of the array. Reproduced with permission from ref. 11, 23, 24 and 45, copyright (2012), (2014), (2017) and (2019) Springer Nature Publishing Group, respectively.

wafers that simultaneously capture the intracellular records of thousands of connected mammalian neurons outside the body. The throughput of the experiment was highlighted by a 19 min recording of over 300 excitatory and inhibitory synaptic connections in more than 1700 neurons. The high-fidelity and simultaneous recording of a large quantity of neuron connection signals is of great significance in electrophysiological research. This can be applied in the electrophysiological screening and improvement of candidate drugs for nervous system diseases (Fig. 12d).[23] The reproducibility of VNW sensors is very important for intracellular signal detection and result verification. According to the previous research progress, the VNW sensors has good repeatability in detecting intracellular information VNW sensors, such as those made with IrO_x electrodes, have been shown to be reliable in repeated experiments due to their high biocompatibility and robust electrodes.

The resistance of nanometer electrode significantly affects intracellular or extracellular biosensing, especially the electrical signals recording. VNW arrays exhibit reliable high performance in detecting intracellular electric signals rather than a single electrode sensor.[12] On the one hand, VNW arrays electrode possesses larger total sensing area than a single micro/nano-wire electrode so that the impedance of the VNW electrode is smaller, in the case of both types of electrodes exhibit similar unit areas impedance. On the other hand, the multiple nanoscale sub-electrodes generate stronger coupling to the cell than the planar or the single micro/nano-wire electrode, which lead to relative high seal resistance between the electrode and the cell membrane.[142] Both low electrode impedance and high seal resistance have been proved to be helpful to enhance the electrical sensing performance.[149] As a result, VWN arrays based biosensors demonstrate great potentials in intracellular electrical signals detecting, as reviewed in this chapter.

5.3 Detection of intracellular biochemical indices

Biochemical indices that including mRNAs, proteins, enzymes and other important biomarkers reflect the life activity rules of living bodies, reveal the essence of life phenomena, and have important significance for regulating and controlling the metabolism and energy transformation of living bodies. In particular, detecting intracellular biochemical indices provides the ability to quantitatively study the changes in substances produced by living cells during biochemical processes, which is greatly helpful for understanding the functions of biological systems.

In the process of studying the expression of proteins and mRNAs and the enzyme activity in cells, factually understanding the technology used in basic biological research, biomedical engineering, and early medical diagnosis is particularly important. Many analysis methods exist, but all of them have their limitations. Routine testing of cell contents requires cell lysis, extraction, and quantification using standard analytical methods such as spectrophotometry, chromatography, mass spectrometry, sequencing, and radiometry. As a result, lysed cells can only be used for one experiment, and the dynamic information cannot be captured. In recent years, some emerging indicator probes, such as fluorescent dyes and functional NPs, have been used to track intracellular activity in real time without lysis of cells.[154,155] However, these probes have limitations in temporal and spatial resolution, and their application is limited by biosafety issues. Nanowire array-based biosensors can be used to extract proteins and mRNAs from cells and detect enzyme activity, which have high medical significance. Yu-ran Na *et al.* reported that the enzyme activity of living cells can be detected by a nanowire sandwich. Living cells were placed between two vertical silicon nanometer arrays, one of which fixed the cells and the other fixed the enzyme substrate; a variety of enzyme activities were simultaneously detected by fluorescence microscopy and mass spectrometry. The function of an enzyme can be studied *in situ* by using a nanometer array sandwich (Fig. 13a).[156]

Inspired by vertically aligned nanowires, Chiappini and coworkers used nanoneedle sensors to detect the cytoplasmic activity of cathepsin B (CTSB, widely used as a biomarker of solid tumors). The sensor consisted of a fluorescently labeled CTSB cutting peptide covalently combined with a nanoneedle array (Fig. 13b). The nanoneedle sensed intracellular activity by connecting to the intracellular environment. The CTSB peptide was cleaved under the action of CTSB and released fluorescence labeling material. The activity of CTSB in cells was then determined by fluorescence microscopy or flow cytometry.[157] Cao *et al.* extracted intracellular proteins and mRNAs using 150 nm nanostraw arrays and analyzed these molecules by fluorescence microscopy, ELISA, and real-time fluorescence quantitative PCR. Forty-one of the 48 analyzed mRNA sequences from human induced pluripotent stem cell cardiomyocytes (hiPSC-CMs) were precisely quantified, and this approach could be applied to CHO cells, hiPSC-CMs cells, and 3D cortical sphere differentiated astrocytes. The extraction process was non-destructive, with a cell survival rate of more than 95% after sampling; cells could be analyzed for a long enough time to understand the processes of induced pluripotency and differentiation (Fig. 13c).[39] Lactate dehydrogenase B (LDHB) is crucial for breaking down glucose in cells to produce energy. LDHB can be used as a biomarker to detect diseases, such as cancer, acute pancreatitis, and AIDS. Hollow nanowires of 450 nm diameter were used to apply a long-term electrical pulse, and intracellular LDHB diffused into the microfluidic channel of the device along with the nanowires (Fig. 13d). LDHB quantitative analysis by ELISA showed repeatability and consistency of protein extraction, which are critical for detecting intracellular protein expression and understanding cell behavior and functions.[81]

Reviewed VNW arrays for intracellular sensing application in this section were summarized in Table 5. Similar design strategies as extracellular sensors including multi-level structural nanowires and top-down processing are employed on the intracellular sensors, for the purpose of better contact/penetration to cell membrane and better mechanical reliability, respectively. The emerging strategies of VNW based intracellular sensors are the utilization of hollow nanowires (nanostraws) and truly individual nanowire-electrode arrays. Hollow nanowires give VNW sensors the ability of both intracellular biosensing and

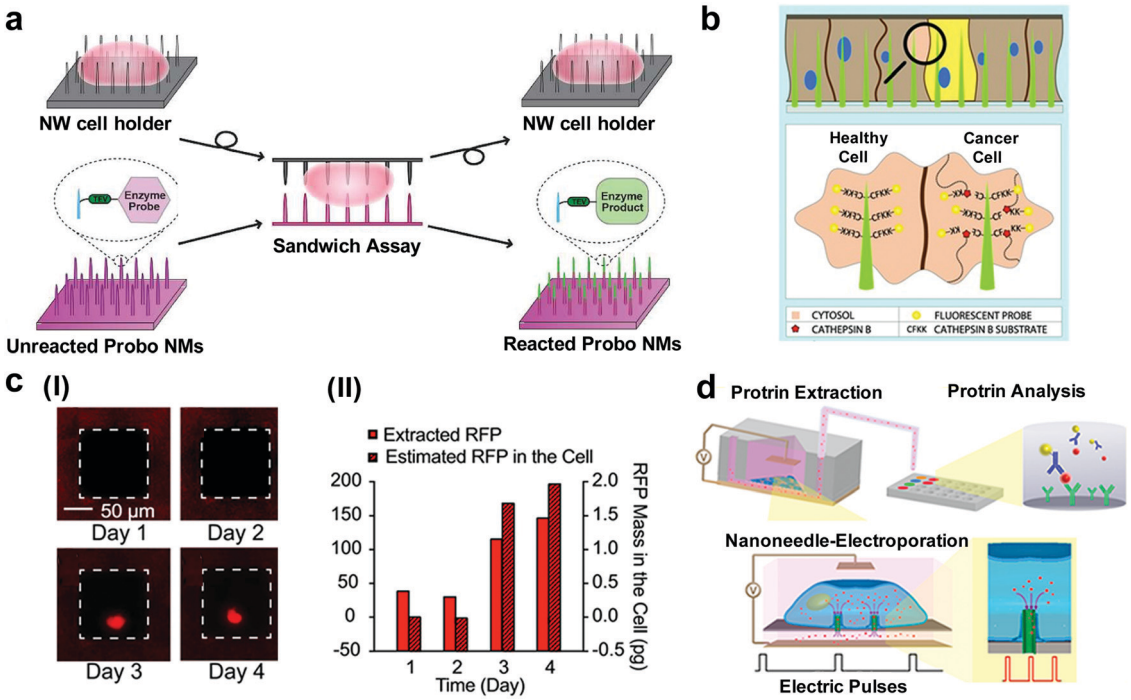

Fig. 13 Detection of intracellular biochemical indicators using VNW arrays. (a) Schematic diagram of intracellular enzyme activity detection by a nanoneedle sandwich. (b) Schematic diagram of the interface between sensors and cells. At the junction, the peptide substrate is cleaved by the active CTSB, releasing fluorescent probes connected to the cytoplasm. (c)-(I) RFP was sampled longitudinally from a CHO cell. The RFP was transfected at sample points on day 2. (II) The calibrated RFP values in cell fluorescence were compared with the extracted RFP values. The amount of extracted RFP increased with increasing intracellular RFP expression. (d) Electroporation of cells with nanoneedles can release proteins from the cells into channels. Proteins are extracted from the channels for ELISA analysis. Reproduced with permission from ref. 39, 81, 156 and 157, copyright (2013) ACS Publishing Group, (2015) Advanced Materials Publishing Group, (2017) Proceedings of the National Academy of Sciences Publishing Group and (2018) American Chemical Society Publishing Group, respectively.

substances transporting that includes drug delivery into cells and extracting substances from cells. Correspondingly, template-assistant deposition procedure and etching are both needed in the device fabrication, rather than direct etching or deposition process applied in most non-hollow nanowires devices. Truly individual nanowire-electrode arrays provide dynamic sub-micron resolution heatmap of intracellular signals of a group of cells, demonstrating an important aspect of intracellular sensing research. And the tactful integration of nanowires fabrication and semiconductor technology provides novel strategy for building up truly individual nanowires devices with significantly reduced complexity. Other strategies such as the selecting of cell penetration methods have been reviewed elsewhere and are not discussed in this review article.[53] All these strategies together with continuous increasing new methodologies impulse the VNW based intracellular sensing a highly active research field.

6. Summary and perspective

The rapid development of VNW arrays has provided a versatile platform in the biosensing field. This review briefly introduces the research advances in VNW array-based biosensors, including the material fabrication principles, device design strategies, cell penetration methodologies, cell interface aspects, and applications. The focus is on the device design strategies of VNW arrays sensors for specific biomedical tasks, including biomolecular sensing, extra/intra-cellular biochemical and electrophysiological signal recording. Design and functionalization of VNW arrays are a prerequisite for high-sensitivity, high-selectivity, high-throughput, and synchronous biosensor detection. First of all, the appearance of VNW arrays facilitate the high performance biomolecular and cellular detection. Further, optimizing the processing approach, structure design and surface functionalization of nanowire arrays can effectively improve the dynamic detection performance of bioactive molecules and regulation of cell behavior. Based on the well designed and fabricated VNW arrays devices, plasma membrane penetration and cytosolic access have been achieved. It promotes VNW arrays towards multifunctional biomedical research platform for noninvasive intra-tissue/cellular biomolecular sampling and dynamic analysis, intracellular drug delivery, electrical signal recording, and *in situ* monitoring/regulating cell transformation, *etc.* These superior analytical tools will provide a higher standard to examine cellular life.

As illustrated throughout this review, advances in VNW array-based biosensors for biomedical applications have led to an unprecedented level of research in life information science. Still, several challenges for VNW array-based biosensors

Table 5 Summary of VNW arrays used for intracellular sensors applications

Material	Geometry	Height (μm)	Diameter (nm)	Fabrication method	Cell type	Penetration mode	Biomedical application	Efficiency[a]	Ref.
Si	Nanowire	~3	100–200	CVD; dry-etching	HeLa, human fibroblasts, NPC (rat neural progenitor cells), primary rat hippocampal neurons	Spontaneous penetration	Delivery of plasmid DNA; siRNA; peptide; protein	>95%	9
Si	Porous nanoneedle	5	50	MACE	HeLa	Spontaneous penetration	Delivery of siRNA	38%	15
Si	Nanocone	3.2	100	DRIE	GPE86, L1.2, Jurkat T, primary mouse T cells	Mechanical force	Delivery of DNA plasmids and siRNA	—	34
Si	Nanowire	3–6	30, 90, 400	CVD	mESCs, HEK293	Spontaneous penetration	Delivery of DNA plasmids	—	14
Si	Nanowire	3–5	100 (tip) 200–400 (base)	Dry-etching	HeLa, PC3	Mechanical force	Probing intracellular enzymatic activity	~88%	15
Si	Porous nanoneedle	5	<50 (tip)	MACE	HET-1A, OE33	Spontaneous penetration	Detection of cytosolic enzymatic activity	~84%	156
Pt	Nanostraw	0.8–3	400 (outer)	Electrodeposition, oxygen RIE	HeLa	Electroporation	Intracellular delivery and sensing	>80%	50
Pt	Nanopillar	1–2	150–200	FIB milling	HL-1	Electroporation	Intracellular recording of action potentials	—	10
Pt	Nanopillar	1	150	FIB milling	Embryonic cortical neutrons	—	Neutron pinning	—	66
SiO_2	Nanopillar	0.7–2	50–350	RIE	NIH3T3, HL-1, MCF-7 primary hippocampal neurons	—	Probing of nuclear mechanics	—	30
SiO_2	Nanopillar	0.7	50–500	EBL, RIE	SK-MEL-2	—	Nanoscale manipulation of membrane curvature	—	146
Al_2O_3	Nanostraw	1–2	100, 250, 750	ALD, O_2-RIE	HeLa, CHO	Spontaneous penetration	Delivery of Co^{2+} ions and GFP plasmid	Co^{2+}, 70%; Alexa Fluor, 40%; pGFP, 5–10%	40 and 41
Al_2O_3	Nanostraw	1.5–2.5	150 (outer)	ALD, O_2-RIE	HEK293, hiPSC-CMs, hESCs, human fibroblasts, mouse primary glia cells, mouse primary neuron cells	Electroporation	GFP and mCherry mRNA transfection, delivery of STIM1 and Cas9 ribonucleoprotein	mRNA, 60–90%; Cas9 RNP, >90%	25
Al_2O_3	Nanostraw	1.5	150 (inner) 250 (outer)	ALD, O_2-RIE	CHO, HeLa	Electroporation	DNA transfection	Plasmid DNA, >67%; PI, >95%	26
Al_2O_3	Nanostraw	1–3	150 (outer)	ALD, O_2-RIE	CHO, hiPSC-CMs	Electroporation	Intracellular mRNA extraction	mRNA, 60–90%	39
ZnO	Spiky nanostraw	1–1.5	300 (inner) 400 (outer)	ALD, O_2-RIE	MCF-7	Electroporation	Regulation and monitoring of intracellular activity	PI, 80%; pGFP, ~70%	44
Au	Nanotube	1.8	150	FIB milling	Rat hippocampal primary neurons, HL-1	Optoporation	Intra/extra-cellular recording of spontaneous action potentials	—	149
Pt/SiO_2	Nanopillar	3	150	EBL, RIE	Primary rat cortical neurons, HEK293	Electroporation	Stimulation and intracellular recording of neurons	—	11
IrO_x	Nanotube	0.5	180	Electrodeposition	Rat HL-1, primary cardiomyocytes	Electroporation	Intracellular measurement of action potential	—	45
GaP	Nanoneedle	1.5, 3.8, 6.7	80	MOVPE	Mouse fibroblasts	—	Cellular behaviors	—	4

[a] Efficiency: in most cases stands for the delivery or transfection efficiency.

remains. (I) Novel materials are still needed in both direct biomolecular sensing and cell related sensing. Au nanoparticles/nanorods dominates the choices as biosensing interfaces, while VNW sensors with others such as 2D materials (f.i. graphene) immobilized as sensing interface are not in-depth investigated. 2D materials with specific electrical, optical and catalytic properties may provide solutions to the alternatives of high sensing performance and the repeatability. On the other hand, present VNW based extra/intra-cellular sensors consist of mainly metal, silicon or metal oxides that are with much higher Young's modulus than cells (GPa *vs.* ~1 to several hundred kPa), even the stiffness of silicone nanowires (several MPa) are several times higher.[158] The remarkable difference in stiffness will prevent the nanowires from seamless combination with cells, resulting in deteriorate sensing performance. Hydrogel is with similar stiffness as cells, then it is believed to be a proper material for cell related biosensing. Recent research has proved the feasibility of extra/intra-cellular electrical signals recording *via* conductive hydrogel micropillar.[144] We believe that further studies on hydrogel nanowires cell sensors would be successful as well and innovate the VNW device design strategy by material selection. (II) Truly individual nanowire-electrode arrays remain to be well developed. Present bulk nanowires sensors have achieved high sensitivity and selectivity, while high-throughput bio-signals recording at cell-dimension scale (submicron to micron scale) requires for a sensing matrix with each submicron electrode functions individually, namely each electrode works in an circuit separately from others. Reported tactful strategy by synthesizing nanowires on CMOS chips provides a promising solution that integrates nanowires with semiconductor technique,[23] which has been dealing with multichannel and high-throughput signal transportation for decades. We are convinced that more researches with similar strategy will appear soon. (III) VNW devices for multifunctional intracellular applications still need exquisite engineering realization. Specific nanowires structures were designed for multifunctional tasks at the beginning, for instance, hollow nanowires are meant to achieve intracellular bio-signals recording, drug delivery and intracellular substances sampling all together. Although present studies only presented single task realization or preliminary dual-task realization,[44,138,159] we are optimistic to foresee the emerging of multifunctional VNW devices with the assistance from microfluidic and integrated circuit technologies. We believe that by continuously exploring the solutions to these challenges, novel VNW array-based biosensor systems will produce significant improvements in understanding disease mechanisms, diagnosing diseases, and developing new potential clinical therapeutic strategies.

Author contributions

The manuscript was written through contributions of all authors. All authors have given approval to the final version of the manuscript.

Conflicts of interest

The authors declare no conflict of interest.

Acknowledgements

The work is supported in part by the National Natural Science Foundation of China (Grant No. 61771498, 61901535, 51805556, 31900954), Guangdong Province Key Area R&D Program (Grant No. 2018B030332001) and Science and Technology Program of Guangzhou, China (Grant No. 201907010038). The authors wish to thank the Youth 1000 Talents Program of China and 100 Talents Program of Sun Yat-Sen University (76120-18821104) and the Open Research Fund of State Key Laboratory of Bioelectronics, Southeast University for supports.

References

1 I. Pupeza, M. Huber, M. Trubetskov, W. Schweinberger, S. A. Hussain, C. Hofer, K. Fritsch, M. Poetzlberger, L. Vamos, E. Fill, T. Amotchkina, K. V. Kepesidis, A. Apolonski, N. Karpowicz, V. Pervak, O. Pronin, F. Fleischmann, A. Azzeer, M. Žigman and F. Krausz, *Nature*, 2020, **577**, 52–59.
2 L. Raj, T. Ide, A. U. Gurkar, M. Foley, M. Schenone, X. Li, N. J. Tolliday, T. R. Golub, S. A. Carr, A. F. Shamji, A. M. Stern, A. Mandinova, S. L. Schreiber and S. W. Lee, *Nature*, 2011, **475**, 231.
3 H. Wang, Z. Gao, X. Liu, P. Agarwal, S. Zhao, D. W. Conroy, G. Ji, J. Yu, C. P. Jaroniec, Z. Liu, X. Lu, X. Li and X. He, *Nat. Commun.*, 2018, **9**, 562.
4 H. Persson, C. Kobler, K. Molhave, L. Samuelson, J. O. Tegenfeldt, S. Oredsson and C. N. Prinz, *Small*, 2013, **9**, 4006–4016.
5 J. A. Frank, M. J. Antonini and P. Anikeeva, *Nat. Biotechnol.*, 2019, **37**, 1013–1023.
6 H. Acaron Ledesma, X. Li, J. L. Carvalho-de-Souza, W. Wei, F. Bezanilla and B. Tian, *Nat. Nanotechnol.*, 2019, **14**, 645–657.
7 R. Parameswaran, J. L. Carvalho-de-Souza, Y. Jiang, M. J. Burke, J. F. Zimmerman, K. Koehler, A. W. Phillips, J. Yi, E. J. Adams, F. Bezanilla and B. Tian, *Nat. Nanotechnol.*, 2018, **13**, 260–266.
8 Y. Jiang, X. Li, B. Liu, J. Yi, Y. Fang, F. Shi, X. Gao, E. Sudzilovsky, R. Parameswaran, K. Koehler, V. Nair, J. Yue, K. Guo, Y. Fang, H.-M. Tsai, G. Freyermuth, R. C. S. Wong, C.-M. Kao, C.-T. Chen, A. W. Nicholls, X. Wu, G. M. G. Shepherd and B. Tian, *Nat. Biomed. Eng.*, 2018, **2**, 508–521.
9 A. K. Shalek, J. T. Robinson, E. S. Karp, J. S. Lee, D. R. Ahn, M. H. Yoon, A. Sutton, M. Jorgolli, R. S. Gertner, T. S. Gujral, G. MacBeath, E. G. Yang and H. Park, *Proc. Natl. Acad. Sci. U. S. A.*, 2010, **107**, 1870–1875.
10 C. Xie, Z. Lin, L. Hanson, Y. Cui and B. Cui, *Nat. Nanotechnol.*, 2012, **7**, 185–190.

11 J. T. Robinson, M. Jorgolli, A. K. Shalek, M. H. Yoon, R. S. Gertner and H. Park, *Nat. Nanotechnol.*, 2012, **7**, 180–184.
12 J. Abbott, T. Ye, D. Ham and H. Park, *Acc. Chem. Res.*, 2018, **51**, 600–608.
13 H. Y. Lou, W. Zhao, Y. Zeng and B. Cui, *Acc. Chem. Res.*, 2018, **51**, 1046–1053.
14 W. Kim, J. K. Ng, M. E. Kunitake, B. R. Conklin and P. Yang, *J. Am. Chem. Soc.*, 2007, **129**, 7228–7229.
15 C. Chiappini, E. De Rosa, J. O. Martinez, X. Liu, J. Steele, M. M. Stevens and E. Tasciotti, *Nat. Mater.*, 2015, **14**, 532–539.
16 E. Lestrell, F. Patolsky, N. H. Voelcker and R. Elnathan, *Mater. Today*, 2019, **33**, 87–104.
17 C. S. Hansel, M. N. Holme, S. Gopal and M. M. Stevens, *Biomaterials*, 2020, **226**, 119406.
18 C. Chiappini, *ACS Sens.*, 2017, **2**, 1086–1102.
19 R. Elnathan, M. Kwiat, F. Patolsky and N. H. Voelcker, *Nano Today*, 2014, **9**, 172–196.
20 T. Berthing, S. Bonde, C. B. Sorensen, P. Utko, J. Nygard and K. L. Martinez, *Small*, 2011, **7**, 640–647.
21 M. E. Spira and A. Hai, *Nat. Nanotechnol.*, 2013, **8**, 83–94.
22 M. Dipalo, V. Caprettini, G. Bruno, F. Caliendo, L. D. Garma, G. Melle, M. Dukhinova, V. Siciliano, F. Santoro and F. De Angelis, *Adv. Biosyst.*, 2019, **3**, 1900148.
23 J. Abbott, T. Ye, K. Krenek, R. S. Gertner, S. Ban, Y. Kim, L. Qin, W. Wu, H. Park and D. Ham, *Nat. Biomed. Eng.*, 2019, **4**, 232–241.
24 J. Abbott, T. Ye, L. Qin, M. Jorgolli, R. S. Gertner, D. Ham and H. Park, *Nat. Nanotechnol.*, 2017, **12**, 460–466.
25 Y. Cao, H. Chen, R. Qiu, M. Hanna, E. Ma, M. Hjort, A. Zhang, R. S. Lewis, J. C. Wu and N. A. Melosh, *Sci. Adv.*, 2018, **4**, eaat8131.
26 X. Xie, A. M. Xu, S. Lealortiz, Y. Cao, C. C. Garner and N. A. Melosh, *ACS Nano*, 2013, **7**, 4351–4358.
27 A. Tay and N. Melosh, *Acc. Chem. Res.*, 2019, **52**, 2462–2471.
28 A. F. McGuire, F. Santoro and B. Cui, *Annu. Rev. Anal. Chem.*, 2018, **11**, 101–126.
29 L. Yan, J. Zhang, C. S. Lee and X. Chen, *Small*, 2014, **10**, 4487–4504.
30 L. Hanson, W. Zhao, H. Y. Lou, Z. C. Lin, S. W. Lee, P. Chowdary, Y. Cui and B. Cui, *Nat. Nanotechnol.*, 2015, **10**, 554–562.
31 S. G. Higgins, M. Becce, A. Belessiotis-Richards, H. Seong, J. E. Sero and M. M. Stevens, *Adv. Mater.*, 2020, **32**, 1903862.
32 C. S. Hansel, S. W. Crowder, S. Cooper, S. Gopal, M. João Pardelha da Cruz, L. de Oliveira Martins, D. Keller, S. Rothery, M. Becce, A. E. G. Cass, C. Bakal, C. Chiappini and M. M. Stevens, *ACS Nano*, 2019, **13**, 2913–2926.
33 F. Tamzalit, M. S. Wang, W. Jin, M. Tello-Lafoz, V. Boyko, J. M. Heddleston, C. T. Black, L. C. Kam and M. Huse, *Sci. Immunol.*, 2019, **4**, eaav5445.
34 Y. Chen, S. Aslanoglou, G. Gervinskas, H. Abdelmaksoud, N. H. Voelcker and R. Elnathan, *Small*, 2019, **15**, 1904819.
35 J. Huang, Y. Zhu, H. Zhong, X. Yang and C. Li, *ACS Appl. Mater. Interfaces*, 2014, **6**, 7055–7762.
36 T. Yasui, S. Rahong, K. Motoyama, T. Yanagida, Q. Wu, N. Kaji, M. Kanai, K. Doi, K. Nagashima, M. Tokeshi, M. Taniguchi, S. Kawano, T. Kawai and Y. Baba, *ACS Nano*, 2013, **7**, 3029–3035.
37 R. Ahmad, N. Tripathy, M. S. Ahn, K. S. Bhat, T. Mahmoudi, Y. Wang, J. Y. Yoo, D. W. Kwon, H. Y. Yang and Y. B. Hahn, *Sci. Rep.*, 2017, **7**, 5715–5724.
38 E. Borberg, M. Zverzhinetsky, A. Krivitsky, A. Kosloff, O. Heifler, G. Degabli, H. P. Soroka, R. S. Fainaro, L. Burstein, S. Reuveni, H. Diamant, V. Krivitsky and F. Patolsky, *Nano Lett.*, 2019, **19**, 5868–5878.
39 Y. Cao, M. Hjort, H. Chen, F. Birey, S. A. Leal-Ortiz, C. M. Han, J. G. Santiago, S. P. Paşca, J. C. Wu and N. A. Melosh, *Proc. Natl. Acad. Sci. U. S. A.*, 2017, **114**, 1866–1874.
40 J. J. VanDersarl, A. M. Xu and N. A. Melosh, *Nano Lett.*, 2012, **12**, 3881–3886.
41 A. M. Xu, A. Aalipour, S. Leal-Ortiz, A. H. Mekhdjian, X. Xie, A. R. Dunn, C. C. Garner and N. A. Melosh, *Nat. Commun.*, 2014, **5**, 3613.
42 B. Tian, T. Cohen-Karni, Q. Qing, X. Duan, P. Xie and C. M. Lieber, *Science*, 2010, **329**, 830–834.
43 J. Abbott, T. Ye, K. Krenek, R. S. Gertner, S. Ban, Y. Kim, L. Qin, W. Wu, H. Park and D. Ham, *Nat. Biomed. Eng.*, 2019, **4**, 232–241.
44 G. He, J. Feng, A. Zhang, L. Zhou, R. Wen, J. Wu, C. Yang, J. Yang, C. Li, D. Chen, J. Wang, N. Hu and X. Xie, *Nano Lett.*, 2019, **19**, 7201–7209.
45 Z. C. Lin, C. Xie, Y. Osakada, Y. Cui and B. Cui, *Nat. Commun.*, 2014, **5**, 3206–3215.
46 X. Liu and S. Wang, *Chem. Soc. Rev.*, 2014, **43**, 2385–2401.
47 S. Rahong, T. Yasui, N. Kaji and Y. Baba, *Lab Chip*, 2016, **16**, 1126–1138.
48 H. Liu, M. Ruan, J. Xiao, Z. Zhang, C. Chen, W. Zhang, Y. Cao, R. He, Y. Liu and Y. Chen, *ACS Appl. Mater. Interfaces*, 2018, **10**, 66–74.
49 Y. J. Hwang, C. Hahn, B. Liu and P. Yang, *ACS Nano*, 2012, **6**, 5060–5069.
50 C. Xie, L. Hanson, Y. Cui and B. Cui, *Proc. Natl. Acad. Sci. U. S. A.*, 2011, **108**, 3894–3899.
51 R. Wen, A. Zhang, D. Liu, J. Feng, J. Yang, D. Xia, J. Wang, C. Li, T. Zhang, N. Hu, T. Hang, G. He and X. Xie, *ACS Appl. Mater. Interfaces*, 2019, **11**, 43936–43948.
52 J. F. Woolley, J. Stanicka and T. G. Cotter, *Trends Biochem. Sci.*, 2013, **38**, 556–565.
53 G. He, N. Hu, A. M. Xu, X. Li, Y. Zhao and X. Xie, *Adv. Funct. Mater.*, 2020, **30**, 1909890.
54 Q. Gao, V. G. Dubrovskii, P. Caroff, J. Wong-Leung, L. Li, Y. Guo, L. Fu, H. H. Tan and C. Jagadish, *Nano Lett.*, 2016, **16**, 4361–4367.
55 S.-i. Kim, H. Yoon, H. Lee, S. Lee, Y. Jo, S. Lee, J. Choo and B. Kim, *J. Mater. Chem. C*, 2015, **3**, 100–106.
56 Z. Huang, N. Geyer, P. Werner, J. de Boor and U. Gosele, *Adv. Mater.*, 2011, **23**, 285–308.
57 H. Wang, M. Sun, K. Ding, M. T. Hill and C. Z. Ning, *Nano Lett.*, 2011, **11**, 1646–1650.

58 R. Juhasz, N. Elfström and J. Linnros, *Nano Lett.*, 2005, **5**, 275–280.
59 T. Mårtensson, P. Carlberg, M. Borgström, L. Montelius, W. Seifert and L. Samuelson, *Nano Lett.*, 2004, **4**, 699–702.
60 A. del Campo and E. Arzt, *Chem. Rev.*, 2008, **108**, 911–945.
61 Z. Huang, H. Fang and J. Zhu, *Adv. Mater.*, 2007, **19**, 744–748.
62 W. Hallstrom, M. Lexholm, D. B. Suyatin, G. Hammarin, D. Hessman, L. Samuelson, L. Montelius, M. Kanje and C. N. Prinz, *Nano Lett.*, 2010, **10**, 782–787.
63 J. Padmanabhan, E. R. Kinser, M. A. Stalter, C. Duncan-Lewis, J. L. Balestrini, A. J. Sawyer, J. Schroers and T. R. Kyriakides, *ACS Nano*, 2014, **8**, 4366–4375.
64 J. Harberts, R. Zierold, C. Fendler, A. Koitmäe, P. Bayat, I. Fernandez-Cuesta, G. Loers, B.-P. Diercks, R. Fliegert, A. H. Guse, C. Ronning, G. Otnes, M. Borgström and R. H. Blick, *RSC Adv.*, 2019, **9**, 11194–11201.
65 H. Kim, H. Jang, B. Kim, M. K. Kim, D. S. Wie, H. S. Lee, D. R. Kim and C. H. Lee, *Sci. Adv.*, 2018, **4**, eaau6972.
66 C. Xie, L. Hanson, W. Xie, Z. Lin, B. Cui and Y. Cui, *Nano Lett.*, 2010, **10**, 4020–4024.
67 C. Ciro, J. O. Martinez, D. R. Enrica, C. S. Almeida, T. Ennio and M. M. Stevens, *ACS Nano*, 2015, **9**, 5500–5509.
68 S. Barth, F. Hernandez-Ramirez, J. D. Holmes and A. Romano-Rodriguez, *Prog. Mater. Sci.*, 2010, **55**, 563–627.
69 A. M. Morales and C. M. Lieber, *Science*, 1998, **279**, 208–211.
70 J. Hu, M. Ouyang, P. Yang and C. M. Lieber, *Nature*, 1999, **399**, 48–51.
71 W. S. Shi, H. Y. Peng, Y. F. Zheng, N. Wang, N. G. Shang, Z. W. Pan, C. S. Lee and S. T. Lee, *Science*, 2000, **12**, 1343–1345.
72 A. I. Hochbaum, R. Fan, R. He and P. Yang, *Nano Lett.*, 2005, **5**, 457–460.
73 V. G. Dubrovskii, G. E. Cirlin, N. V. Sibirev, F. Jabeen, J. C. Harmand and P. Werner, *Nano Lett.*, 2011, **11**, 1247–1253.
74 A. Zhang and C. M. Lieber, *Chem. Rev.*, 2015, **116**, 215–257.
75 B. Tian and C. M. Lieber, *Chem. Rev.*, 2019, **119**, 9136–9152.
76 Y. Wu and P. Yang, *J. Am. Chem. Soc.*, 2001, **123**, 3165–3166.
77 A. Ganapathi, P. Swaminathan and L. Neelakantan, *ACS Appl. Nano Mater.*, 2019, **2**, 5981–5988.
78 W. Lee and S.-J. Park, *Chem. Rev.*, 2014, **114**, 7487–7556.
79 C. Schönenberger, B. M. I. van der Zande, L. G. J. Fokkink, M. Henny, C. Schmid, M. Krüger, A. Bachtold, R. Huber, H. Birk and U. Staufer, *J. Phys. Chem. B*, 1997, **101**, 5497–5505.
80 H. Mukaibo, *Chem. Rec.*, 2019, **19**, 859–872.
81 G. He, C. Yang, T. Hang, D. Liu, H. J. Chen, A. H. Zhang, D. Lin, J. Wu, B. R. Yang and X. Xie, *ACS Sens.*, 2018, **3**, 1675–1682.
82 Y. Bahari Mollamahalle, M. Ghorbani and A. Dolati, *Electrochim. Acta*, 2012, **75**, 157–163.
83 J. Xu, N. Xu, X. Zhang, P. Xu, B. Gao, X. Peng, S. Mooni, Y. Li, J. Fu and K. Huo, *Sens. Actuators, B*, 2017, **244**, 38–46.
84 T. Ozel, B. A. Zhang, R. Gao, R. W. Day, C. M. Lieber and D. G. Nocera, *Nano Lett.*, 2017, **17**, 4502–4507.
85 R. Liu, R. Chen, A. T. Elthakeb, S. H. Lee, S. Hinckley, M. L. Khraiche, J. Scott, D. Pre, Y. Hwang, A. Tanaka, Y. G. Ro, A. K. Matsushita, X. Dai, C. Soci, S. Biesmans, A. James, J. Nogan, K. L. Jungjohann, D. V. Pete, D. B. Webb, Y. Zou, A. G. Bang and S. A. Dayeh, *Nano Lett.*, 2017, **17**, 2757–2764.
86 F. Zhang, Y. Jiang, X. Liu, J. Meng, P. Zhang, H. Liu, G. Yang, G. Li, L. Jiang, L.-J. Wan, J.-S. Hu and S. Wang, *Nano Lett.*, 2016, **16**, 766–772.
87 M. Lin, J. F. Chen, Y. T. Lu, Y. Zhang, J. Song, S. Hou, Z. Ke and H. R. Tseng, *Acc. Chem. Res.*, 2014, **47**, 2941–2950.
88 M. Jamal, J. Xu and K. M. Razeeb, *Biosens. Bioelectron.*, 2010, **26**, 1420–1424.
89 S. Yan, N. He, Y. Song, Z. Zhang, J. Qian and Z. Xiao, *J. Electroanal. Chem.*, 2010, **641**, 136–140.
90 D. H. Kwon, H. H. An, H.-S. Kim, J. H. Lee, S. H. Suh, Y. H. Kim and C. S. Yoon, *Appl. Surf. Sci.*, 2011, **257**, 4650–4654.
91 Y. Lu, S. Peng, D. Luo and A. Lal, *Nat. Commun.*, 2011, **2**, 578–583.
92 Z. Zhang, Y. Xie, Z. Liu, F. Rong, Y. Wang and D. Fu, *J. Electroanal. Chem.*, 2011, **650**, 241–247.
93 S. Su, X. Wei, Y. Zhong, Y. Guo, Y. Su, Q. Huang, S.-T. Lee, C. Fan and Y. He, *ACS Nano*, 2012, **6**, 2582–2590.
94 Q. Yan, Z. Wang, J. Zhang, H. Peng, X. Chen, H. Hou and C. Liu, *Electrochim. Acta*, 2012, **61**, 148–153.
95 S. W. Han, S. Lee, J. Hong, E. Jang, T. Lee and W. G. Koh, *Biosens. Bioelectron.*, 2013, **45**, 129–135.
96 P. Serre, C. Ternon, V. Stambouli, P. Periwal and T. Baron, *Sens. Actuators, B*, 2013, **182**, 390–395.
97 C. W. Hsu and G. J. Wang, *Biosens. Bioelectron.*, 2014, **56**, 204–209.
98 M. Long, L. Tan, H. Liu, Z. He and A. Tang, *Biosens. Bioelectron.*, 2014, **59**, 243–250.
99 D. P. Neveling, T. S. van den Heever, W. J. Perold and L. M. T. Dicks, *Sens. Actuators, B*, 2014, **203**, 102–110.
100 S. Rahong, T. Yasui, T. Yanagida, K. Nagashima, M. Kanai, A. Klamchuen, G. Meng, Y. He, F. Zhuge, N. Kaji, T. Kawai and Y. Baba, *Sci. Rep.*, 2014, **4**, 5252.
101 C.-W. Hsu, W.-C. Feng, F.-C. Su and G.-J. Wang, *J. Electrochem. Soc.*, 2015, **162**, B264–B268.
102 C. Yang, C. Chen, Y. Pan, S. Li, F. Wang, J. Li, N. Li, X. Li, Y. Zhang and D. Li, *Electrochim. Acta*, 2015, **182**, 264–271.
103 S. Rahong, T. Yasui, T. Yanagida, K. Nagashima, M. Kanai, G. Meng, Y. He, F. Zhuge, N. Kaji and T. Kawai, *Anal. Sci.*, 2015, **31**, 153–157.
104 S. Rahong, T. Yasui, T. Yanagida, K. Nagashima, M. Kanai, G. Meng, Y. He, F. Zhuge, N. Kaji, T. Kawai and Y. Baba, *Sci. Rep.*, 2015, **5**, 10584.
105 J. Kim, S. Y. Park, S. Kim, D. H. Lee, J. H. Kim, J. M. Kim, H. Kang, J. S. Han, J. W. Park, H. Lee and S. H. Choi, *Sci. Rep.*, 2016, **6**, 31984.
106 J. Lee, M. H. Hong, S. Han, J. Na, I. Kim, Y. J. Kwon, Y. B. Lim and H. J. Choi, *Nanoscale Res. Lett.*, 2016, **11**, 341.

107 F. Yu, Y. Li and L. Tang, *Optik*, 2016, **127**, 11492–11496.
108 X. Wen, M. Long and A. Tang, *J. Electroanal. Chem.*, 2017, **785**, 33–39.
109 T. Yasui, T. Yanagida, S. Ito, Y. Konakade, D. Takeshita, T. Naganawa, K. Nagashima, T. Shimada, N. Kaji, Y. Nakamura, I. A. Thiodorus, Y. He, S. Rahong, M. Kanai, H. Yukawa, T. Ochiya, T. Kawai and Y. Baba, *Sci. Adv.*, 2017, **3**, e1701133.
110 Y. Zhang, T. Jiang and L. Tang, *Biosens. Bioelectron.*, 2017, **97**, 278–284.
111 B. Chakraborty, S. Ghosh, N. Das and C. RoyChaudhuri, *Biosens. Bioelectron.*, 2018, **122**, 58–67.
112 X. Gong, Y. Gu, F. Zhang, Z. Liu, Y. Li, G. Chen and B. Wang, *Front. Mater.*, 2019, **6**, DOI: 10.3389/fmats.2019.00003.
113 S. Rafique, S. Khan, S. Bashir and R. Nasir, *Chem. Pap.*, 2019, **74**, 229–238.
114 R. K. Saiki, S. Scharf, F. Faloona, K. B. Mullis, G. T. Horn, H. A. Erlich and N. J. S. Arnheim, *Science*, 1985, **230**, 1350–1354.
115 Z. Y. Jiang, X. X. Jiang, S. Su, X. P. Wei, S. T. Lee and Y. He, *Appl. Phys. Lett.*, 2012, **100**, 203104.
116 T. Yasui, T. Yanagida, T. Shimada, K. Otsuka, M. Takeuchi, K. Nagashima, S. Rahong, T. Naito, D. Takeshita, A. Yonese, R. Magofuku, Z. Zhu, N. Kaji, M. Kanai, T. Kawai and Y. Baba, *ACS Nano*, 2019, **13**, 2262–2273.
117 J. Zhang, D. Han, R. Yang, Y. Ji, J. Liu and X. Yu, *Bioelectrochemistry*, 2019, **128**, 126–132.
118 S. W. Han, S. Lee, J. Hong, E. Jang, T. Lee and W. G. Koh, *Biosens. Bioelectron.*, 2013, **45**, 129–135.
119 N. V. Klassen, D. Marchington and H. C. McGowan, *Anal. Chem.*, 1994, **66**, 2921–2925.
120 L. Blonde, M. Merilainen, V. Karwe, P. Raskin and T. S. Group, *Diabetes, Obes. Metab.*, 2009, **11**, 623–631.
121 E. A. Moschou, B. V. Sharma, S. K. Deo and S. Daunert, *J. Fluoresc.*, 2004, **14**, 535–547.
122 L. Yuan, W. Lin, Y. Xie, B. Chen and S. Zhu, *J. Am. Chem. Soc.*, 2011, **134**, 1305–1315.
123 D. T. Bostick and D. M. Hercules, *Anal. Chem.*, 1975, **47**, 447–452.
124 S. Hanaoka, J.-M. Lin and M. Yamada, *Anal. Chim. Acta*, 2001, **426**, 57–64.
125 R. F. P. Nogueira, M. C. Oliveira and W. C. Paterlini, *Talanta*, 2005, **66**, 86–91.
126 K.-i. Yamakoshi and Y. Yamakoshi, *J. Biomed. Opt.*, 2006, **11**, 054028.
127 G.-C. Zhao, Z.-Z. Yin, L. Zhang and X.-W. Wei, *Electrochem. Commun.*, 2005, **7**, 256–260.
128 C. Shan, H. Yang, J. Song, D. Han, A. Ivaska and L. Niu, *Anal. Chem.*, 2009, **81**, 2378–2382.
129 W. Kim, S. H. Lee, S. H. Kim, J. C. Lee, S. W. Moon, J. S. Yu and S. Choi, *ACS Appl. Mater. Interfaces*, 2017, **9**, 5891–5899.
130 Y. Q. Li, B. K. Chandran, C. T. Lim and X. Chen, *Adv. Sci.*, 2015, **2**, 1500118.
131 B. J. Green, T. Saberi Safaei, A. Mepham, M. Labib, R. M. Mohamadi and S. O. Kelley, *Angew. Chem., Int. Ed.*, 2016, **55**, 1252–1265.
132 H. Liu, Y. Li, K. Sun, J. Fan, P. Zhang, J. Meng, S. Wang and L. Jiang, *J. Am. Chem. Soc.*, 2013, **135**, 7603–7609.
133 X. Liu, L. Chen, H. Liu, G. Yang, P. Zhang, D. Han, S. Wang and L. Jiang, *NPG Asia Mater.*, 2013, **5**, e63.
134 L. Wu, X. Xu, B. Sharma, W. Wang, X. Qu, L. Zhu, H. Zhang, Y. Song and C. Yang, *Small Methods*, 2019, **3**, 1800544.
135 S. Wang, H. Wang, J. Jiao, K. J. Chen, G. E. Owens, K. Kamei, J. Sun, D. J. Sherman, C. P. Behrenbruch, H. Wu and H. R. Tseng, *Angew. Chem., Int. Ed.*, 2009, **48**, 8970–8973.
136 S. Wang, K. Liu, J. Liu, Z. T. Yu, X. Xu, L. Zhao, T. Lee, E. K. Lee, J. Reiss, Y. K. Lee, L. W. Chung, J. Huang, M. Rettig, D. Seligson, K. N. Duraiswamy, C. K. Shen and H. R. Tseng, *Angew. Chem., Int. Ed.*, 2011, **50**, 3084–3088.
137 G. S. Park, H. Kwon, D. W. Kwak, S. Y. Park, M. Kim, J. H. Lee, H. Han, S. Heo, X. S. Li, J. H. Lee, Y. H. Kim, J. G. Lee, W. Yang, H. Y. Cho, S. K. Kim and K. Kim, *Nano Lett.*, 2012, **12**, 1638–1642.
138 G. He, C. Yang, J. Feng, J. Wu, L. Zhou, R. Wen, S. Huang, Q. Wu, F. Liu, H.-J. Chen, T. Hang and X. Xie, *Adv. Funct. Mater.*, 2019, **29**, 1806484.
139 G. He, J. Feng, A. Zhang, L. Zhou, R. Wen, J. Wu, C. Yang, J. Yang, C. Li, D. Chen, J. Wang, N. Hu and X. Xie, *Nano Lett.*, 2019, **19**, 7201–7209.
140 M. Voelker and P. Fromherz, *Small*, 2005, **1**, 206–210.
141 A. Hai, J. Shappir and M. E. Spira, *Nat. Methods*, 2010, **7**, 200–202.
142 A. Hai, A. Dormann, J. Shappir, S. Yitzchaik, C. Bartic, G. Borghs, J. P. Langedijk and M. E. Spira, *J. R. Soc., Interface*, 2009, **6**, 1153–1165.
143 E. W. Keefer, B. R. Botterman, M. I. Romero, A. F. Rossi and G. W. Gross, *Nat. Nanotechnol.*, 2008, **3**, 434–438.
144 Y. Liu, A. F. McGuire, H.-Y. Lou, T. L. Li, J. B.-H. Tok, B. Cui and Z. Bao, *Proc. Natl. Acad. Sci. U. S. A.*, 2018, **115**, 11718–11723.
145 M. T. Yang, N. J. Sniadecki and C. S. Chen, *Adv. Mater.*, 2007, **19**, 3119–3123.
146 P. Paulitschke, F. Keber, A. Lebedev, J. Stephan, H. Lorenz, S. Hasselmann, D. Heinrich and E. M. Weig, *Nano Lett.*, 2019, **19**, 2207–2214.
147 W. Zhao, L. Hanson, H. Y. Lou, M. Akamatsu, P. D. Chowdary, F. Santoro, J. R. Marks, A. Grassart, D. G. Drubin, Y. Cui and B. Cui, *Nat. Nanotechnol.*, 2017, **12**, 750–756.
148 V. Caprettini, J.-A. Huang, F. Moia, A. Jacassi, C. A. Gonano, N. Maccaferri, R. Capozza, M. Dipalo and F. De Angelis, *Adv. Sci.*, 2018, **5**, 1800560.
149 L. Hanson, Z. C. Lin, C. Xie, Y. Cui and B. Cui, *Nano Lett.*, 2012, **12**, 5815–5820.
150 M. Dipalo, H. Amin, L. Lovato, F. Moia, V. Caprettini, G. C. Messina, F. Tantussi, L. Berdondini and F. De Angelis, *Nano Lett.*, 2017, **17**, 3932–3939.
151 Y. Zhao, S. S. You, A. Zhang, J.-H. Lee, J. Huang and C. M. Lieber, *Nat. Nanotechnol.*, 2019, **14**, 783–790.
152 R. Kawamura, M. Miyazaki, K. Shimizu, Y. Matsumoto, Y. R. Silberberg, R. R. Sathuluri, M. Iijima, S. Kuroda,

F. Iwata, T. Kobayashi and C. Nakamura, *Nano Lett.*, 2017, **17**, 7117–7124.

153 X. Duan, R. Gao, P. Xie, T. Cohen-Karni, Q. Qing, H. S. Choe, B. Tian, X. Jiang and C. M. Lieber, *Nat. Nanotechnol.*, 2011, **7**, 174–179.

154 L. Wang, M. S. Frei, A. Salim and K. Johnsson, *J. Am. Chem. Soc.*, 2019, **141**, 2770–2781.

155 A. B. Chinen, C. M. Guan, J. R. Ferrer, S. N. Barnaby, T. J. Merkel and C. A. Mirkin, *Chem. Rev.*, 2015, **115**, 10530–10574.

156 Y. R. Na, S. Y. Kim, J. T. Gaublomme, A. K. Shalek, M. Jorgolli, H. Park and E. G. Yang, *Nano Lett.*, 2013, **13**, 153–158.

157 C. Chiappini, P. Campagnolo, C. S. Almeida, N. Abbassi-Ghadi, L. W. Chow, G. B. Hanna and M. M. Stevens, *Adv. Mater.*, 2015, **27**, 5147–5152.

158 H. Yuk, B. Lu and X. Zhao, *Chem. Soc. Rev.*, 2019, **48**, 1642–1667.

159 A. Cerea, V. Caprettini, G. Bruno, L. Lovato, G. Melle, F. Tantussi, R. Capozza, F. Moia, M. Dipalo and F. De Angelis, *Lab Chip*, 2018, **18**, 3492–3500.

